Data assimilation of realistic generic boundary-layer flows for wind-turbine applications - An LES study

Linus Wrba¹, Antonia Englberger¹, Andreas Dörnbrack¹, Gerard Kilroy¹, and Norman Wildmann¹ Deutsches Zentrum für Luft- und Raumfahrt, Institut für Physik der Atmosphäre, Oberpfaffenhofen, Germany **Correspondence:** Linus Wrba (linus.wrba@dlr.de)

Abstract. Providing observed date- and site-specific turbulent inflow fields for large-eddy simulations (LES) of the flow through wind turbines becomes increasingly important for realistic reliable estimates of power production. In this study, data assimilation techniques are applied to adapt the atmospheric inflow field towards measurement data. A previously defined wind profiles. A standard and a modified version of the Newtonian relaxation technique and a vibration assimilation method an assimilation method based on the vibration equation are implemented in the geophysical flow solver EULAG. The extent to which they are able to adapt mean wind profiles to field measurements and simultaneously maintain the horizontal wind velocities towards target profiles and the impact on atmospheric turbulence of an idealized LES is are investigated. The sensitivity of the methods to grid refinement and to parameter changes is analysed. The vibration assimilation technique is better-method based on the vibration equation is suited for fine grids $(\frac{dx}{dx} = \frac{dy}{dy} = \frac{dz}{dz} = 5)$ m) because of smaller damping effects on the atmospheric turbulence., which are necessary in wind-energy applications. Furthermore, the vibration method is used to nudge the inflow field zonal and meridional inflow velocities of an idealized atmospheric simulation towards velocity profiles measured representing a weakly-stably-stratified atmospheric boundary layer (ABL) at the wind-farm site WiValdi at Krummendeich, Germany. A case with nearly neutral therman stratification in the atmospheric boundary layer is chosen from the measurements to test the assimilation technique. The oscillation assimilation method On site wind measurements and the output of mesoscale simulations are evaluated to define the target velocity profile. The assimilation method based on the vibration equation is able to adapt the zonal and meridional velocity components of an atmospheric flow . The LESs applying data assimilation are compared with the measurements and independent mesoscale simulations. A good accordance is found for the mean inflow velocity profiles and the turbulence intensities, while damping effects on the atmospheric turbulence could be reduced. In a final step, the assimilated flow field is taken as inflow for a wind-turbine simulation, which then shows the characteristic structures of a wake in the atmospheric boundary layer ABL. This study demonstrates that an efficient computing of different and realistic shows the suitability of the vibration assimilation technique for adapting inflow fields for wind-turbine simulations is possible applying the vibration assimilation wind energy purposes and presents the advantages and disadvantages of the method.

25

45

50

1 Introduction

The growing demand for wind energy is accompanied with a wide range of challenges as structural components and technical characteristics of wind turbines are getting more and more sophisticated. Especially, the interaction of wind turbines In particular, the mutual interaction of wind-turbine wakes in wind farms and their response to the transient atmospheric flow field are grand challenges in wind energy research (cf. Veers et al., (2023)), wind-energy research (cf. Veers et al., 2023). General attention is laid on the performance paid to the performance of the turbines and the loads on the blades which are mainly controlled by the turbulence in the ABL (cf. Hansen (2013), Wharton and Lundquist (2012)). The crucial question is , how much power can be harvested (cf. Hansen, 2013; Wharton and Lundquist, 2012). The general question is how to maximize the harvested power of a wind turbine at a certain location with a specific configuration of wind turbines. The atmospheric situation during which under specific operational conditions. One of the decisive factors in answering this question is the atmospheric situation under which the wind turbines are operatinghas to be involved in such considerations. Knowledge of the thermal stratification and the flow conditions is becoming increasingly important because rotor diameters and are getting larger and the hub heights are increasing and cover a wide getting higher, thus covering a greater depth of the ABL. A better knowledge of the impact of different atmospheric characteristics like the vertical gradient of the horizontal velocity and turbulence intensities on the wake behind impacting a wind turbine and its wake is therefore essential, especially for wind parks with multiple turbines, Either field measurements or numerical simulations can provide the required information about the flow field surrounding a rotor. The recent opening of the research wind park WiValdi¹ (Wind Validation) in Krummendeich, North Germany on 15 August 2023 by the German Aerospace Center (DLR) and the Research Alliance Wind Energy (FVWE²) offers a timely opportunity to expand our knowledge on this topic. The wind park consists of two Enercon E-115 EP3 turbines with hub heights of 92 m and rotor diameters of D = 116 m separated by a rather narrow spacing of 4.4 D. In addition, a smaller custom-built turbine is currently under construction. The flow fields and the turbine wakes at the wind park can be measured in great detail by the vast observational network located on site. This network includes a series of measuring masts, multiple Doppler wind lidar (DWL) instruments, and a microwave radiometer.

Even with a really dense observational network and a large number of field measurements that can provide quasi-reliable 3-D pictures of the atmospheric situation, there are still natural spatial and temporal limitations in resolving all motion modes affecting the response of wind turbines to the atmospheric flow. In order to close such scale gaps, numerical simulations can provide 3-D flow fields of the entire wind park with very high spatial and temporal resolutions. In particular, LES models have been proven a useful to be a useful and powerful tool to compute these turbulent flow fields. In contrast to simulations based on Reynolds-averaged Navier-Stokes (RANS) equations, LESs are capable of resolving turbulence partially in the flow. In

¹https://windenergy-researchfarm.com

²Forschungsverbund Windenergie https://www.fvwe.uni-oldenburg.de

addition, LESs are computationally less expensive than direct numerical simulations (DNS) because the subgrid-scale (SGS) subgrid-scale (SGS) contribution to the turbulence is parameterized.

LESs are widely used in literature in order to assess the impact of the atmospheric stratification on also frequently used to evaluate the effects of thermal stratification of the ABL on the wakes of wind turbines and wind farms. The beginnings of for various atmospheric conditions (cf. Bhaganagar and Debnath, 2014; Abkar et al., 2016; Vollmer et al., 2016; Englberger and Dörnbrack, 2

1. Particular emphasis has been placed on a distinctive thermal ABL stratification (neutral, convective, stable) on the flow around a single wind turbine and the flow in a wind farm (Porté-Agel et al., 2020). However, the majority of these studies conduct their basic research with idealized LESs for the purpose of meteorological applications lay in the 1960s and 1970s (e.g. Lilly (1965) and Deardorff (1974)). With the increasing importance of wind power for the energy sector, wind turbines have been included frequently in (cf. Porté-Agel et al. (2020)). Troldborg et al. (2007) revealed that a higher atmospheric turbulence leads to a more rapid wake recovery. Further research considered the differences in the flow during the diurnal cycle. The behavior of the wake for a stable stratified nighttime boundary layer has been investigated numerically by e.g. Lu and Porté-Agel (2011), Bhaganagar and Debnath (2014, 2015) and Abkar and Porté-Agel (2015) as well as for the diurnal cycle (cf. Abkar et al. (2016) and Englberger and Dörnbrack (2018)). These studies show a less rapid wake recovery under stable conditions during night than under convective conditions during day.

There are different numerical approaches for the generation of turbulent inflow fields for wind-turbine simulations. One possibility are synthetic turbulence fields which were proposed by Mann (1994). With these stochastic models high computational costs can be avoided but they are not physical models in a sense that they satisfy the conservation laws (cf. Naughton et al. (2011)

). Atmospheric inflow fields which are more close to reality are generated by s. Idealized atmospheric flow simulations which are computed without a wind turbine are often used to provide inflow fields for in wind-turbine simulations (cf. Bhaganagar and Debnath (2014), Abkar et al. (2016), Englberger and Dörnbrack (2017)). These atmospheric precursor simulations are computationally expensive because turbulence has to spin up in the regarded domain until the key flow parameters (vertical gradient of horizontal velocity, turbulence intensity) match anticipated characteristics in the . Furthermore, most of these simulations are conducted for idealized flow conditions in , that are characterized by no large- and mesoscale forcing and by no temporal or spatial variation of the and often deviate from actual atmospheric situations. This is a disadvantage for a reliable prediction of the energy gain at a certain location because the loads on the blades are very sensitive to mesoscale inflow conditions, for example orographically induced deviations from these idealized inflow. Realistic associated pressure gradient. The representation of real, measured flow conditions like those observed in WiValdi, however, cannot be addressed reliably with such purely idealized setups.

One way to generate site-specific three-dimensional simulations are necessary for the analysis of wind energy plants for varying flow regimes. However, it is still challenging to simulate regional or local flow fields by . One option for the generation of site-specific atmospheric inflow conditions is the coupling of flow conditions is to couple mesoscale simulations (e.g. simulations of the Weather Research and Forecasting Model (WRF)) with the microscale simulation (LES). Recent experience on (Skamarock et al., 2019)) with LESs (e.g., Aitken et al., 2014; Sanchez Gomez and Lundquist, 2020; Kilroy et al., 2024). Recent advances in this research field has been made in by the Mesoscale to Microscale Coupling (MMC) project spon-

sored by the U.S. Department of Energy (cf. Haupt et al., (2022)). The authors are emphasizing (cf., Haupt et al., 2022). There, the authors emphasize the complexity of modeling the correct energy transfer from the largest scales of the atmosphere to those scales inside motion to the scales within the ABL where wind turbines extract energy, Simulations from which the wind turbines generate electrical energy. Further, they note that simulations from the mesoscale down to the microscale (for example with. with the mentioned WRF-LES) are very computational expensive. The consideration of wind and temperature observations in s would be a logical way to introduce realistic data into high-resolution simulations of turbulent flow. However, it is quite challenging to run simulations accounting for all previously defined conditions (initial conditions, surface boundary conditions, large-scale forcing) to match the observed flow parameters (cf. Allaerts et al. (2023)). Detailed observational data from atmospheric situations is also spatially and temporally limited. Furthermore, site-specific measurements show in general similar flow characteristics for one stratification and a main wind direction and only small differences in the hub-height wind speed, the vertical gradient of the velocity and the atmospheric turbulence. Data Assimilation is a possibility to keep simulated flow parameters like windspeed and potential temperatureclose to measurement data. In the model (cf. Skamarock et al. (2019)) different four-dimensional data assimilation schemes developed by Stauffer and Seaman (1990) are implemented. Concerning microscale simulations, an advantage of this approach would be coupling) are computationally exceptionally expensive. Therefore, such elaborate methods cannot be used to simulate a variety of different atmospheric situations, assuming that both the computing time and the physical time required to perform the simulations are far too long.

100

105

110

115

120

An alternative approach to circumvent the expensive meso- and microscale coupling is to conduct idealized numerical simulations coupled with a suitable data-assimilation method for providing date- and site specific turbulent flow conditions.

This numerical approach is computationally less expensive. In such a setup, the combination of the resolved data-assimilation method is assumed to transfer the given mesoscale information (wind and stability profiles) onto the microscale (cf., Stauffer and Seaman, 1

In general, those methods apply a damped harmonic oscillator (often referred to as proportional and integral controller) as an additional forcing in the governing equations of motion. Commonly, this forcing term can consist of a damping (proportional) and an oscillating (integral) part (e.g., Spille-Kohoff and Kaltenbach, 2001). In the case of Newtonian relaxation, only the damping part is considered. Here, the numerically calculated profiles of wind, temperature, humidity etc. are adjusted to given target profiles (which can either come from measurements or are extracted from the output of mesoscale model simulations) using a specific relaxation time scale, which is a free parameter of this method.

The relaxation time scale should be long enough (~ hours) that the small-scale turbulence in the LES with real data observed at specific locations. However, there are some difficulties when data assimilation methods are used in high resolved simulations. The methods have usually damping effects on the atmospheric turbulence due to the averaged variables which are used for the assimilation and do not account for fluctuations. Neggers et al. (2012) and Maronga et al. (2015) noted that the use of the is not affected by it, however, it needs to be small enough to be able to adapt the LES towards mesoscale characteristics in a reasonable time (Neggers et al., 2012). An issue, however, is that turbulence intensity is often overly reduced using Newtonian relaxation. To circumvent this limitation, the damping term has been modified in Allaerts et al. (2020) and Allaerts et al. (2023). Their modified Newtonian relaxation method (often called nudging) implies a relaxation timescale to be large enough to

allow turbulence development but also small enough for an adequate forcing. Allaerts et al. (2020) recently developed the profile-assimilation technique which consists of a proportional gain controller taking as input the time-height history of mean-flow quantities. Nakayama and Takemi (2020) developed an advanced assimilation technique uses an internal forcing technique deduced from mesoscale variables (wind speed and temperature), including the time and height history of these variable in the LES. They tested the approach with the damping part, and a combination of both damping and oscillating, with quite similar results.

Another data-assimilation technique described in Nakayama and Takemi (2020) is based on the vibration equation for the velocity oscillating around a zero-wind basic state with a certain frequency. They pointed out the oscillating part only, which has the property of fluctuating around the target mean values. This integral forcing is controlled by the natural frequency of the flow field, which has to be set appropriately in order not to damp turbulent fluctuations. We refer to this method in the following as the vibration method. Nakayama and Takemi (2020) empahized the advantage of this method in terms of turbulence intensity handling. With this study we want to make a step towards more realistic date- and site-specific inflow fields for handling the turbulence intensity in comparison to the local Newtonian damping.

135

140

145

150

155

While the method of Allaerts et al. (2020) has been directly developed for wind-turbine applications, the method of Nakayama and Taken has been applied only at a rather coarse resolution of 40 m horizontally and relaxes only the horizontal wind field. However, the application of this method to high-resolution wind turbines would have the advantage that it can reproduce an assimilation of simultaneous measurements, is not limited to horizontal homogeneity and can be applied in complex terrain. Therefore, it also seems well-suited for wind-energy applications. Considering the DLR wind-farm WiValdi, it seems to be a worthwhile endeavor to modify the method of Nakayama and Takemi (2020) so that it can be applied to assimilate more realistic observed wind profiles, with the aim of calculating more complex inflow cases that retain realistic turbulent characteristics.

An LES s using data assimilation techniques. This will lead to a better knowledge of wakes behind wind turbines in less idealized and more realistic conditions and wind farm provider will be able to predict the energy gain and the loads at the rotor blades more precisely using the developed methods. The main objective of this study is the computational efficient generation of realistic of a wind turbine or a wind farm, which is conducted with open lateral boundary conditions, requires, in addition to the input of the mesoscale information as horizontal mean values of the corresponding profiles, a turbulent inflow field, which synchronously feeds turbulence in the inflow region. There are different numerical approaches for generating the required turbulent inflow fields, especially for wind-turbine simulations (e.g., Bhaganagar and Debnath, 2014; Abkar et al., 2016; Englberger and D., One possibility is the generation of synthetic turbulence fields, as proposed by Mann (1994). These stochastic models avoid high computational costs but they are not physical models in a sense that they satisfy the conservation laws (cf. Naughton et al., 2011). Turbulent atmospheric inflow fields with arbitrary velocity profiles based on observational data for wind turbines in which are more close to observations are generated by LESs. Measurement data from the research wind farm site WiValdi (https://windenergy-research com/) at Krummendeich in the North of Germany and averaged profiles will be used for a comparative analysis. Therefore, another possibility is the production of a limited amount of idealized precursor simulations, representing specific atmospheric

conditions (neutral, convective, stable). These atmospheric precursor simulations are computationally expensive because turbulence has to spin up in the domain of interest until key flow parameters (vertical gradient of horizontal velocity, turbulence ki-

netic energy (TKE)) match anticipated characteristics in the ABL. Therefore, one main positive effect of the method of Nakayama and Takemi (2020) could be the application of one precursor simulation towards a variety of measurements (occurring under relatively similar atmospheric conditions, for example stratification, geostrophic winds, etc).

The main goal of this work is the application and assessment of the vibration method in wind-energy research. Since the method can use the measured horizontal wind as a background profile, it offers a cost-effective way to simulate the effects of specific atmospheric properties on the wake of wind turbines with high spatial resolution.

The following outstanding scientific questions will be considered:

165

175

180

190

- 4 Which of the considered assimilation method is able to preserve turbulence?
- 2 Can velocities taken from idealized atmospheric precursor simulations be assimilated towards arbitrary measured wind profiles?
- 170 3 How does the wake behind a wind turbine change between idealized and more realistic inflow conditions?

The outline of this publication paper is as follows. The numerical model EULAG, the considered assimilation Newtonian relaxation methods, the measurements and the setup for the precursor simulations vibration assimilation method, the measurements, and the numerical setup are presented in Sect. Section 2. In Sect. 3the Newtonian relaxation and the assimilation technique with the vibration equation are compared for the idealized example presented by Nakayama and Takemi (2020) with dx=dy=40 m and dy=10 m. Subsequently in Sect. 4, both assimilation methods are tested for a finer grid spacing (dx=dy=dz=5 m) and differences compared to the coarse case are examined. In Sect. 5 a site specific inflow field is computed for the wind farm site WiValdiby assimilation of an idealized precursor flow field. In Sect. 6 the assimilation of a precursor simulation is combined with the simulation of the Section 3, we perform idealized LESs to reproduce the results of the coarse-resolution method of Nakayama and Takemi (2020). Section 4 adapts this vibration method towards a wind-energy relevant fine-resolution for their NBL case. Here, we test the applicability of the vibration method at fine resolution and compare it to the performance of both Newtonian approaches. A special focus is on turbulence characteristics, which would offer an answer to our first research question:

Q1 Which of the assimilation methods used is able to preserve turbulence within the scope of the defined conditions?

As our final aim is to simulate real atmospheric situations, which for example may include veering inflows, Section 5 exemplifies how the idealized approach can be modified towards the reproduction of a measured situation in the wind park WiValdi. Here, we focus on the parameter space of the vibration approach and the importance of a proper precursor simulation and use a combination of measurements and a WRF simulation for creating background wind profiles. The results of this investigation allows us to answer our second research question:

Q2 Can velocities taken from precursor simulations of idealized atmospheric flows be assimilated towards arbitrary measured wind profiles?

Finally, we test the applicability of the vibration method in a wind-turbine simulation in Section 6, answering the third research question:

- Q3 How does the wake behind a wind turbine . Conclusions are given in Sect. change if velocities of idealized inflow conditions are assimilated?
- 195 Conclusions are then drawn in Section 7.

2 Methodology

200

205

2.1 The Numerical Model EULAG

The dry and incompressible atmospheric flow as well as the flow through a wind turbine are modelled flow inside the ABL is simulated with the geophysical flow solver EULAG (Prusa et al., 2008). EULAG is an established computational model which is has been used for a wide range of physical scenarios(cf. Prusa et al. (2008)). It has been used for the: The simulation of urban flows (Smolarkiewicz et al., (2007)), gravity waves (Smolarkiewicz and Dörnbrack (2008)), (Smolarkiewicz et al., 2007), of internal gravity waves (Mixa et al., 2021; Dörnbrack, 2024), of turbulent atmospheric flows (Margolin et al., (1999)) and even solar convection (Elliott and Smolarkiewicz (2002))(Margolin et al., 1999), and even for the simulation of solar convection (e.g., Elliott and Smolarkiewicz, 2002). The name EULAG refers to the two possible ways to solve the equations of motion either in EUlerian(flux form) (cf. Smolarkiewicz and Margolin (1993)), i.e. flux form (Smolarkiewicz and Margolin, 1993) or in semi-LAGrangian(advective form) (cf. Smolarkiewicz and Pudykiewicz (1992)) mode., i.e. advective form (Smolarkiewicz and Pudykiew. The advective terms in the fluid equations are approximated by the iterative finite-difference algorithm MPDATA (multidimensional positive definite advection transport algorithm) which is second-order accurate, positive definite, conservative, and computationally efficient (cf. Smolarkiewicz and Margolin (1998)). (Smolarkiewicz and Margolin, 1998). A detailed explanation of EULAG can be found in Smolarkiewicz and Margolin (1998) and Prusa et al. (2008).

For the simulations in this study, the following set of non-hydrostatic Boussinesq equations with constant density $\rho_0 = 1.1 \rho_0 = 1.1 \text{ kg n}$ are solved for the Cartesian velocity components v = (u, v, w) v = (u, v, w) and for the potential temperature perturbation $\Theta' = \Theta - \Theta_e$ (cf. Smolarkiewicz et al. (2007) and Englberger and Dörnbrack (2018)):

 $\Theta' = \Theta - \Theta_e$, see Smolarkiewicz et al. (2007) in general and Englberger and Dörnbrack (2018) for wind-turbine applications:

$$\nabla \cdot \boldsymbol{v} = 0_{\underline{\hspace{0.5cm}}},\tag{1}$$

$$\frac{d\mathbf{v}}{dt} = \underbrace{-\nabla(\frac{p'}{\rho_0})}_{\text{pressure gradient}} + \underbrace{\mathbf{g}\frac{\Theta'}{\Theta_0}}_{\text{buoyancy}} - \underbrace{2\Omega(\mathbf{v} - \mathbf{v}_e)}_{\text{Coriolis-Force }\mathbf{F}_{\text{cor}}} + \underbrace{\frac{\mathbf{F}}{\rho_0}}_{\mathbf{F}_{WT}} - \mathbf{f} + \mathbf{V} + \underbrace{\alpha(\mathbf{v} - \mathbf{v}_e)}_{\mathbf{F}_{abs}}, \tag{2}$$

$$\frac{d\Theta'}{dt} = -\mathbf{v}\nabla\Theta_{e} + \mathbf{H} + \beta\Theta'_{-}.$$
(3)

215

In these equations Θ_0 denotes the constant reference value of the potential temperature and Θ_e the balanced ambient is its balanced ambient/environment state. The operators $\frac{d}{dt}$, ∇ and ∇ represent the total derivative, the gradient and the divergence. p' symbolizes the pressure perturbations, $\mathbf{g} = (0,0,-g)$ $\mathbf{g} = (0,0,-g)$ is the acceleration due to gravity and \mathbf{F}_{cor} indicates the Coriolis force with the angular velocity vector of the earthEarth's rotation Ω . \mathbf{V} and \mathbf{H} are The Coriolis parameter is $f = 1.0 \times 10^{-4} \, \mathrm{s}^{-1}$ for midlatitudes and \mathbf{v}_e is the background velocity.

The SGS terms and \mathbf{V} and \mathbf{H} indicate turbulent dissipation of momentum and diffusion of heat, respectively. The simulations within this study are all conducted with a TKE closure (cf. Margolin et al. (1999)). (Margolin et al., 1999). \mathbf{F}_{abs} is an absorber to reduce fluctuations at the lateral and model top boundaries. A similar absorber is used in the Eq. 3, where α and β are inverse time scales. \mathbf{f} denotes the additional forcing due to data assimilation. In the simulations with wind turbines the selected data assimilation techniques as presented in Section 2.2, see Eqs. 4, 6, and 7.

In the simulation with a wind turbine, \mathbf{F}_{WT} corresponds to the forces generated by the rotor blades. The wind turbine is implemented with the blade-element momentum theory as a rotating actuator disc (ef. Mirocha et al. (2014); Englberger and Dörnbrack (2017). (Mirocha et al., 2014). Unfortunately, the blade data for the Enercon E-115 EP3 turbine necessary for the calculation of the forces on the flow induced by the blades is at the moment not available for the currently not available. The Enercon E-115 EP3 ($h_{hub} = 92 \text{ m}$, rotor diameter D = 116 m) which is built in Krummendeichturbines at the DLR wind park WiValdi have a hub height of $h_{hub} = 92 \text{ m}$ and a rotor diameter D = 116 m. Therefore, the simulations are simulation is conducted with the blade data of the 5 MW reference wind turbine defined by the National Renewable Energy Laboratory (NREL) (Jonkman et al. (2009)) (Jonkman et al., 2009). This wind turbine was selected, as it has a similar hub height ($h_{hub} = 90 \text{ h}_{hub} = 90 \text{ m}$) and a rotor diameter (D = 126 D = 126 m).

2.2 Assimilation Methods

230

235

240

245

250

There are several factors limiting the accuracy and comparability of LESs with real case measurements and field observations. On the one hand, the truncation errors due to discretization which are necessary for the calculation of the solution are limiting the limit the accuracy of the numerical model (ef. Arcucci et al. (2017); Neggers et al. (2012)). (e.g., Arcucci et al., 2017; Neggers et a

In order to resolve this issue, data assimilation techniques of the simulated flow field towards observational data are widely used in many numerical models in order to improve simulation accuracy and for the assimilation of the flow field of the

simulations towards observational dataenhance the realism of LESs. For example, in a the grid-nudging method is implemented based on the four-dimensional data assimilation developed by Stauffer and Seaman (1990). This scheme relies on the definition of the Newtonian relaxation a local Newtonian relaxation according to Eq. 6 of Nakayama and Takemi (2020):

$$\frac{\delta\Phi}{\delta t} \underbrace{NUD} \underbrace{\mathbf{f}_{N}(x, y, z, t)}_{NUD} = -\frac{\Phi - \Phi_{target}}{\tau} damp(x) \rho_{0} \underbrace{\mathbf{v}(x, y, z, t) - \mathbf{v}_{OBS}(z, t)}_{T} \quad \underline{.}$$

$$(4)$$

In this equation Φ is a variable like velocity, temperature or concentration and Φ_{target} symbols its target value with

260

265

280

$$damp(x) = \sin^2\left[\frac{\pi}{2}\left(1 - \frac{x_{\text{nud}} - x}{x_1}\right)\right] \quad , \quad x_{\text{nud}} - \frac{x_l}{2} \le x \quad \le x_{nud} + \frac{x_l}{2} \quad . \tag{5}$$

In Eq. 4, \mathbf{f}_N symbolizes the forcing term \mathbf{f} in the momentum conservation Eq. 2 for the local Newtonian relaxation, \mathbf{v} is the instantaneous velocity vector at a certain grid point, and \mathbf{v}_{OBS} is the vector of the target velocity values given through observational data. τ is the In this study, we consider only the relaxation of the zonal and meridional velocity components.

The Gaussian damping function damp(x) acts only in the zonal direction to prevent numerical artefacts at the borders of the nudging area. x_{nud} is the center of nudging area and x_1 the length of the damping layer in the zonal direction. The relaxation time scale which τ has to be chosen small enough to generate a considerable forcing towards the target data but not too small that small-scale atmospheric turbulence is suppressed (cf. Neggers et al. (2012); Maronga et al. (2015)). The severe drawback of this method is (cf. Neggers et al., 2012; Maronga et al., 2015). Newtonian relaxation according to Eq. 4, which is introduced in Eq. 2, can provoke the damping of small-scale turbulent structures in the atmosphere ABL which is mentioned by Neggers et al. (2012), Maronga et al. (2015), Heinze et al. (2017), Nakayama and Takemi (2020), and Nakayama and Takemi (2020).

A modification of the local Newtonian relaxation of Eq. 4 is applied by (e.g., Maronga et al., 2015; Heinze et al., 2017; Allaerts et al., 2018; Heinze et al., 2018; Hei

$$\mathbf{f}_{\langle N \rangle}(x, y, z, t) = damp(x) \rho_0 \frac{\langle \mathbf{v} \rangle(z, t) - \mathbf{v}_{OBS}(z, t)}{\tau} \quad . \tag{6}$$

Here, a profile $\langle v \rangle$ is computed as a spatial average over the nudging zone, see Eq. 5. Relaxation according to Eq. 4 is referred to as Newtonian relaxation following Allaerts et al. (2020). There, they pointed out that this approach strongly overestimates the simulated TKE during daytime. A comparison of both versions of the Newtonian relaxation for the assimilation of an idealized neutral boundary layer (NBL) is presented in Section 3.

Nakayama and Takemi (2020) proposed a different way of assimilating velocities in LESs based on the vibration equation for the velocity oscillating around a zero-wind basic state with a certain frequency. They showed that their method preserves turbulent fluctuations well and can still approximate velocities to measured wind profiles. The following forcing term $\mathbf{f}_{\mathcal{K}}$ is derived from the vibration equation

$$\mathbf{f}(x,y,z,t) = damp(x)\rho_0\omega_0^2 \int_0^t (u(x,y,z,t') - U_{OBS}(z,t'))dt'$$

with

$$damp(x) = \sin^2\left[\frac{\pi}{2}\left(1 - \frac{x_{\text{nud}} - x}{x_l}\right)\right] \quad , \quad x_{\text{nud}} - \frac{x_l}{2} \le \quad x \quad \le x_{nud} + \frac{x_l}{2} \quad .$$

fsymbolizes the forcing term additionally introduced in the equation for the conservation of momentum following Nakayama and Takemi (Eq. 2). u and U_{OBS} correspond to the instantaneous wind velocity at a certain grid point and the averaged observational velocity at the related height, respectively. ρ is the density and ω_0 the 7):

$$\mathbf{f}_{V}(x,y,z,t) = damp(x) \rho_{0} \omega_{0}^{2} \int_{0}^{t} \left(\mathbf{v}(x,y,z,t') - \mathbf{v}_{OBS}(z,t') \right) dt' \quad . \tag{7}$$

Here, $\omega_0 = 2\pi f_0$ is the frequency for the oscillating velocity in the vibration equation $\frac{1}{2\pi} damp(x)$ is a Gaussian damping function in the streamwise direction to prevent numerical artefacts at the borders of the nudging area. x_{nud} is the center of nudging area in and x_1 the length of the damping layer for the streamwise direction, which has to be set smaller than the peak frequency in the energy spectrum of the precursor simulation. We refer to this method in the following as the vibration method.

2.3 Measurement Data

Since November 2020, a long-range, scanning DWL is has been installed at the WiValdi site to measure vertical profiles of wind speed and direction over the entire height of the ABL. The DWL is configured to measure in a velocity azimuth display (VAD) mode with a high angular resolution and a specific elevation angle to obtain accurate measurements of the mean wind vector profile as well as TKE and its dissipation rate (Wildmann et al. (2020))(Wildmann et al., 2020). A microwave radiometer is has also been installed along-side to obtain temperature and humidity profilesas well. With this combination of instruments, long-term statistics and typical characteristics of atmospheric conditions at the site can be determined (Wildmann et al. (2022)). For the comparison of the assimilated velocities in the (Wildmann et al., 2022).

In Section 5, the zonal and meridional velocity components of an idealized precursor simulation in Sect. 5, as situationwas chosen the 19.11.2021 18 UTC to are assimilated towards more complex target profiles corresponding to one measured situation. A 10 min time average profile covering the period from 1830 UTC to 1840 UTC of 19 UTC November 2021 was selected, which features strong wind shear near to the ground and a larger large wind veer in the boundary layer. ABL under weakly stably stratified conditions (confirmed by analysing observed vertical temperature profiles taken from the microwave radiometer). As continuous measurements are only available from z = 57 m up to z = 470 m, a simulation with WRF was performed for this period and continuous velocity profiles were generated. The WRF setup and the generation of the used target profiles is described in appendix A. Figure 1 shows the measured velocity profiles \overline{u}_{DWL} and \overline{v}_{DWL} and the continuous profiles from the WRF simulations \overline{u}_{WRF} and \overline{v}_{WRF} .

2.4 Precursor Simulations

305

310

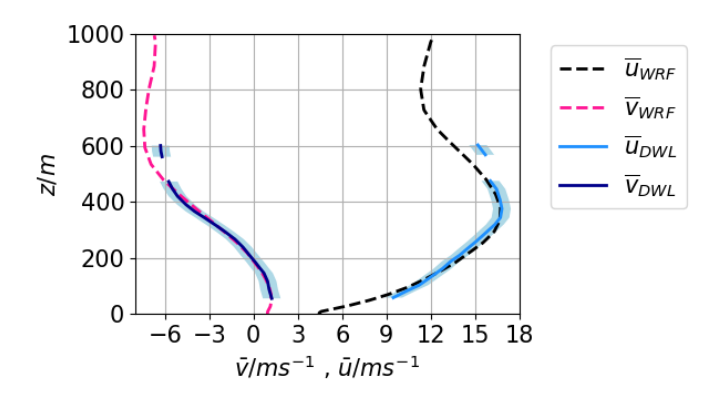


Figure 1. Vertical profiles of the measured velocities at the WiValdi site (zonal \overline{u}_{DWL} , meridional \overline{v}_{DWL}) and the continuous profiles from the WRF simulations (zonal \overline{u}_{WRE} , meridional \overline{v}_{WRE}).

The numerical simulations are separated into a precursor simulation and a simulation with data assimilation (+ wind turbine simulation). Table

2.4 Numerical Setup

Table 1 gives an overview of all simulations which are conducted during performed in this study. Figure 2 shows a schematic illustration of the simulation approach used in this study. In the first precursor simulation. The numerical simulations are separated into precursor simulations (P1, P2, P3 in Fig. 2) and simulations with data assimilation (N1, <N1>, V1, N2, <N2>, V2, SO in Fig. 2) (+ wind turbine simulations, SW and SOW in Fig. 2). A precursor simulation is necessary so that characteristic atmospheric turbulence can spin up in the computational domain. The precursor simulations P1, P2, and P3 employ periodic
 lateral boundary conditions and are run until a fully developed turbulent state prevails. In the subsequent simulations, in which the output of the precursor simulations is used as the inflow field, either the local Newtonian relaxation according to Eq. 4 (N1, N2), the Newtonian relaxation according to Eq. 6 (<N1>, <N2>), or the vibration method using Eq. 7 (V1, V2, SO) are applied.

Our numerical simulations N1, <N1>, and V1 have a similar setup as those of Nakayama and Takemi (2020). N1 and V1 and are conducted to verify the correct implementation of our assimilation methods, <N1> to compare with Allaerts et al. (2020). The sensitivity of the different assimilation methods to grid refinement is evaluated with the simulations N2, <N2>, and V2. The assimilation towards more complex target profiles for the zonal and meridional velocity components is tested in the simulation SO. As mentioned above, these profiles are close to observations at the wind farm site WiValdi (Fig. 1). While we have tested different Newtonian relaxation timescales (τ = 30 s, τ = 60 s and τ = 300 s) and different vibration frequencies (f₀ = 0.002 s⁻¹, f₀ = 0.005 s⁻¹ and f₀ = 0.01 s⁻¹), in this study only the results for τ = 30 s and f₀ = 0.002 s⁻¹ are shown. These particular values led to the closest alignment with the target profile.

Idealized cases - coarse resolution (P1, N1, <N1>, V1)

335

345

350

355

360

In the precursor simulation P1, a fully developed flow corresponding to $\frac{1}{4}$ an NBL with the zonal velocity profile $\frac{1}{4} = \frac{1}{4} \cdot \left(\frac{z}{z_0}\right)^n u = \frac{u_*}{k!} \ln\left(\frac{z}{z_0}\right)$ (friction velocity $\frac{1}{4} = 0.45u_* = 0.45u_* = 0.45$ m s⁻¹, roughness length $\frac{z_0}{z_0} = 0.1$ mand exponent $n = 0.14z_0 = 0.1$ m, von Karman constant $\kappa = 0.4$) is achieved by the application of a constant pressure gradient in the horizontal direction. following Nakayama and Takemi (2020). In Fig. 2, P1 refers to this precursor simulation. The pressure gradient is implemented as an additional forcing $-u_*^2/H$ in Eq. 2 with the above friction velocity and the domain height $\frac{1}{H} = \frac{1000 H}{150000} = \frac{1000 m}{150000}$ m. For the surface friction the drag coefficient in the surface parametrization parameterization is set to 0.017. 150000 time steps with $\Delta t = 1$ s are calculated on 100 processors in 25 physical hours for this precursor simulation to develop an equilibrium. For the comparison to the investigation of Nakayama and Takemi (2020) the domain size was identically set to which is a requirement of EULAG's Neumann boundary conditions. The domain size is $6000 \times 6000 \times 1000 \times 10000 \times 10000 \times 10000 \times$

The precursor simulation is performed with periodic boundary conditions in the horizontal directions and an open boundary condition rigid lid at the top of the domain. The Coriolis-parameter is set to zero. For the following simulation with data assimilation, synchronized 2D yz-slices are extracted at x = 3000x = 3000 m at each time step after the simulation has reached a quasi-equilibrium state. A total of 1050 2D slices from of the three velocity components and the potential temperature perturbation were taken as input at the inlet of the nudging simulation. Here, the boundary conditions in the horizontal directions and at the top are open, the additional pressure gradient term is excluded and the accelerations due to earth rotation are turned on.

The nudging simulations N1, <N1> and V1 are calculated with periodic boundaries in the meridional y-direction, an open boundary condition at the zonal outflow in the x-direction, and a gradient-free, rigid-lid upper boundary. The Coriolis term in Eq. 2 is omitted in the nudging simulations, which is different to the setup of Nakayama and Takemi (2020). An explanation for this difference is given in Section 3. A nudging zone is introduced from x = 1.0-2.0 km over the whole lateral and vertical span of the computational domain. A logarithmic zonal target wind profile with $u_* = 0.41$ m s⁻¹ and $z_0 = 0.2$ m is assumed, while the meridional target wind profile is set to 0. The three assimilation methods (Eq. 4, 6, 7) are tested separately for the adaption towards the zonal target profile in N1, <N1> and V1 respectively. Numerical absorbers (the term \mathbf{F}_{abs} in Eq. 2) are included at the top above z = 700 m and at the outflow for x > 5000 m in order to reduce numerical boundary effects.

Idealized cases - fine resolution (P2, N2, <N2>, V2)

As wind-turbine simulations require a higher resolution we performed another a precursor simulation P2 for the same NBL conditions like as in P1. The grid spacing for this simulation is dx with a grid spacing of dx = dy - dy = dz - dz = 5 m. A smaller domain is chosen in order to reduce the calculation time and it is set to 3000 x. The time step has to be decreased to $\Delta t = 0.2$ s and a smaller domain of $6000 \times 3000 \times 1000$ m³ is chosen in order to reduce the calculation time. The boundary conditions in horizontal direction remain periodic and the remain the same as in the coarse-grid equivalent. Only the drag coefficient is decreased to 0.01 to fit for the velocity profile prescribed by the power law in P1. At the top of the domain the boundary

condition is open. Due to the smaller time step, a total of 6000 synchronized 2D yz-slices are extracted from this precursor simulation for the input of the nudging simulation. The presented precursor simulations are used for the assessment of the different assimilation methods which are explained in Sect. 2.2.A simulations N2, <N2> and V2. With this high-resolved inflow the performance of the assimilation techniques Eqs. 4, 6, 7 can be investigated. All other settings in N2, <N2> and V2, not referred to in this paragraph, are identical to N1, <N1> and V1.

370 Real cases (P3, SO, SOW, SW)

In Section 5 a more complex target profile is implemented which has a zonal and a meridional component close to the measurements at the wind-farm site WiValdi (Fig. 1). Therefore, a third precursor simulation P3 is assessed in this study to test the assimilation technique conducted with wind shear and veer in the ABL flow. The atmospheric condition in this simulation corresponds to a stable stratification. This precursor simulation was developed by Englberger and Dörnbrack (2018) during their investigation of the impact of different thermal stratifications on wind-turbine wakes. The domain size of this in the simulations applying the precursor simulation P3 is $5120 \times 2560 \times 320 \text{ m}^3$ with a grid spacing of dx= $\frac{\text{dy}}{\text{dy}}$ = $\frac{\text{dz}}{\text{dz}}$ = $\frac{\text{dz$ the two different assimilation techniques are applied for different setups according to Tab. 1. Similar to Nakayama and Takemi (2020) a nudgingzone is introduced from x = 2.5 - 3.5 km over the whole lateral and vertical span in the computational domain with the coarse grid spacing. An idealized target wind profile with a power-law exponent of n = 0.25 is assumed following the example of Nakayama and Takemi (2020). For the simulations with the fine grid spacing the nudging area is situated from x = 0.5 - 1.5 km in order to have enough space between the nudging zone and the horizontal outflow boundary at x = 3 km for the investigation of the flow. In the the nudging zone ranges from x = 2.0 - 3.0 km. simulation SO with nudging, the nudging zone is inserted at x = 1.0-2.0 km and an absorber is included for x > 4520 m (no damping at domain top). In the corresponding wind-turbine simulation SOW the NREL 5 MW rotor is placed 200 m downstream of the nudging zone. The calculation time of the wind-turbine simulation is 60 min with an averaging period of the velocities of 20 min at the end of the simulation. A reference simulation SW with the wind turbine is computed with the original precursor P3 as inflow without an assimilation approach.

The assimilation methods described in Section 2.2 are only suitable if the domain averaged mean flow of the precursor simulation corresponds to the domain averaged target value. This is required to preserve mass continuity (Eq. 1) in the numerical model. If there is a difference between the precursor and the target velocity profile, the horizontal mean of the vertical profile of the precursor simulation has to be normalized:

$$v_i^{new}(x,y,z) = \alpha \langle \overline{v}_i^p(z) \rangle_{x,y} + v_i^{\prime p}(x,y,z)$$
(8)

with

375

380

385

390

$$\alpha = \frac{\langle v_{i,OBS} \rangle_z}{\langle \overline{v}_i^P \rangle_{x,y,z}} \quad . \tag{9}$$

Here, v_i^{new} is the new velocity value of the inflow field at every grid point, $\langle \overline{v}_i^p(z) \rangle_{x,y}$ is the spacial $(\langle \rangle_{x,y})$ and time-averaged mean value at every height of the precursor simulation and $v_i^{\prime p} = v_i^p - \langle \overline{v}_i^p(z) \rangle_{x,y}$ is the fluctuation at every grid point i,j,k

of the precursor simulation. α is derived from the division of the mean of the target profile $\langle v_{i,QBS} \rangle_z$ (averaged over the height of the ABL) by the time and volume-averaged mean velocity (averaged over the last 20 min) of the precursor simulation $\langle \overline{v}_i^P \rangle_{x,y,z}$.

Name	Precursor Simulation	Assimilation method	Grid Resolution	Target Profile
N1	P1	local Newton	coarse	idealized n=0.25
<u><n1></n1></u>	P1	Newton	coarse	idealized
V1	P1	Vibration	coarse	idealized n=0.25
N2	P2	local Newton	fine	idealized n=0.25
V2 < <u>N2</u> >	P2	Vibration Newton	fine	idealized n=0.25
₩ <mark>₩</mark>	P2	Vibration	fine	observation-idealized
so	Р3	Vibration	fine	observation_WiValdi
sow	Р3	Vibration	fine	observation WiValdi + wind turbine
<u>SW</u>	<u>P3</u>	-~	fine	wind turbine

Table 1. Simulations conducted in this study.

400 3 Validation of the implemented Assimilation Method

In-

405

410

2.1 ABL and wind-turbine characteristics

In this work the following characteristics of the first part of this section the results of the Newtonian relaxation method (Eq. ??) in N1 are shortly presented. In the second part the numerical results with the application of the assimilation method using the vibration equation (Eq. ?) in V1 are shown. The results of the two implemented methods are compared to the investigations of Nakayama and Takemi (2020). According to the computational setup in Nakayama and Takemi (2020) the basic turbulent boundary layer flow P1 is generated (cf. Sect. ?.4). For the nudging zone a target wind profile with an exponent of n = 0.25 is assumed. The spanwise velocity is approximately zero in ABL are investigated:

- The mean vertical profiles of the zonal $(\langle u(x_a, z) \rangle_y)$ and meridional velocities $(\langle v(x_a, z) \rangle_y)$ are calculated at each height level at certain downstream positions x_a averaged in the y-direction $\langle z \rangle_y$.
- The resolved mean TKE of the ABL

$$< TKE(x_{a}, z) >_{y} = \frac{1}{2} < (< u^{'}(x_{a}, y, z)^{2} >_{y} + < v^{'}(x_{a}, y, z)^{2} >_{y} + < w^{'}(x_{a}, y, z)^{2} >_{y}) >_{y}$$

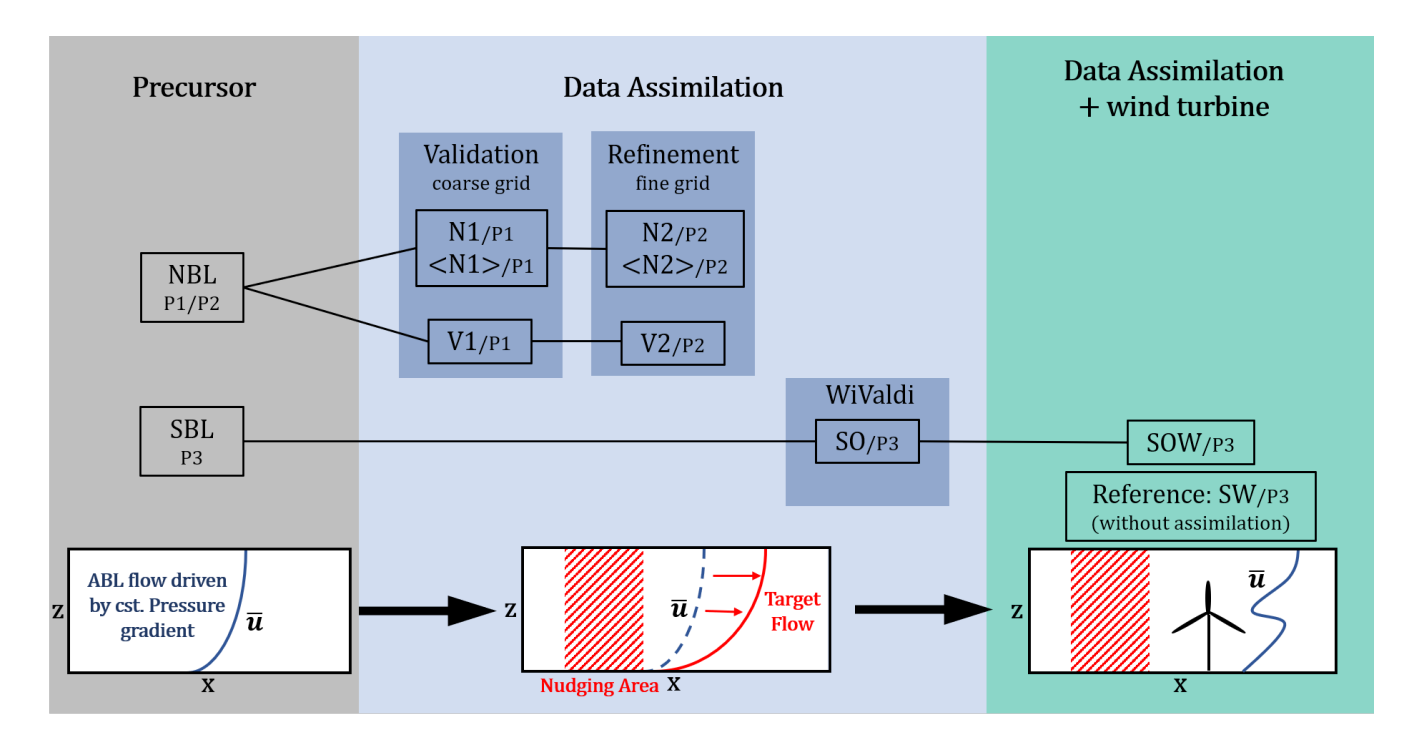


Figure 2. Schematic illustration of the different simulations considered in this study. The abbreviations indicate the simulation type following Table 1.

(10)

is calculated at each height level at certain downstream position x_a averaged in the y-direction $<>_y, u', v'$ and w' are the turbulent fluctuations of the velocity components u, v and w. The fluctuations are calculated subtracting the y-averaged mean velocities from the instantaneous value at each height level. Here, $\chi'(x_a, y, z) = \chi(x_a, y, z) - \langle \chi(x_a, z) \rangle_y$ with $\chi = (u, v, w)$.

- The horizontal energy spectrum is calculated according to Stull (Stull, 2003, Ch. 8.6).

Concerning the wind-turbine simulations in Sect. 6 the time-averaged zonal velocity component $\overline{u_{i,j,k}}$ is shown which is averaged over the last 20 min of the simulation. The zonal velocity deficit is calculated with

$$VD_{i,j,k} \equiv \frac{\overline{u_{1,j,k}} - \overline{u_{i,j,k}}}{\overline{u_{1,j,k}}}$$
 (11)

Here, $\overline{u_{1,i,k}}$ corresponds to the first grid point in x-direction at i = 1.

3 Results: Data Assimilation with coarse-grid Resolution

415

420

In this section the test scenario proposed by Nakayama and Takemi (2020) with a grid spacing of dx = dy = 40 m and dz = 10 m is reproduced in EULAG with the three different assimilation techniques described above. The aim of this section is to verify that there are no major differences in the numerical results and that EULAG is able to reproduce the precursor simulation and is not changed in the nudging zone. In general, the compared simulations are in good accordance to the findings of Nakayama and Takemi (2020).

3.1 Results of the Newtonian Relaxation Method

425

430

435

440

445

450

455

In the first part of this section the results of the Newtonian relaxation method in N1 are shortly presented. The Newtonian relaxation technique is used to calculate the foreing towards the target velocity profile. As described in section 2.2, the foreing acts from 2.5 km to 3.5 km in the streamwise direction and drives the velocity towards the desired wind profile. Figure ?? shows the streamwise mean velocity \overline{u} over the height for different relaxation times inside the nudging zone in a) (2.5-3.5 km) and behind the nudging zone in b) (4-5 km) averaged over the last 20 min of the simulation. The black line refers to the upstream atmospheric flow and the gray dotted line shows the target wind profile. The foreing The results with coarse resolution are also necessary to enable a comparison with the results with a finer grid (Section 4) and they are a verification for our numerical setup without Coriolis force, which differs from Nakayama and Takemi (2020).

The results of both types of Newtonian relaxations (Eq. 4 and Eq. 6) and the assimilation method using the vibration equation (Eq. 7) are shown in Fig. 3. Vertical profiles of the zonal velocity and the resolved TKE at different downstream positions are presented. The zonal velocity component is adapted precisely towards the target profile is clearly visible. For a smaller relaxation time $\tau = 30$ s the amplitude of the forcing is larger and therefore the velocity is better adjusted to the target profile. For $\tau = 30$ s and $\tau = 60$ s an overestimation is apparent behind the nudging zone and the velocity tends back to its original state. The mean velocity is only slightly changed for the relaxation time $\tau = 300$ s. The results are comparable to Fig. for the two options of the Newtonian relaxation (Fig. 3a and b). A slight overestimation of the target velocity profile by less than 0.5 m s⁻¹ can be seen for the simulation with the vibration method (Fig. 3c). In all simulations, the flow downstream of the nudging zone does not change considerably at the positions x = 2 km, x = 3 km and x = 4 in Nakayama and Takemi (2020) and the samedependence on τ is seen. The lower panels of Fig. ?? show the streamwise which is compared for the different simulations. The is set in relation to data of Engineering Science Data Unit (ESDU) 85020 which provides turbulence characteristics of a neutrally stratified related to a smooth surface roughness (cf.Nakayama and Takemi (2020)). Inside the nudging domain a strong decay of the turbulence intensity is perceived for a small relaxation time compared to the atmospheric flow-km. The meridional velocity component is approximately zero in the precursor simulation . Only 35% of the turbulence intensity is preserved at a height of z = 200 mwhich is within the rotor area of modern wind turbines. Downstream of the nudging area the shave recovered well in these simulations. The results for the Newtonian Relaxation method in Nakayama and Takemi (2020) and is not changed inside the nudging zone (not shown).

Regarding the TKE, a strong damping to values below $0.05 \text{ m}^2 \text{ s}^{-2}$ can be seen at all heights shown when the local Newtonian relaxation according to Eq. 4 is applied (Fig.4)and in this study are similar for higher relaxation time scales. For small time scales, the numerical simulation with EULAG leads to a faster returning to the original turbulence intensity downstream of the

nudging area than the code LOHDIM-LES developed by Nakayama et al. (2012, 2014, 2016). We assume that the differences for the regarding small relaxation time scales are due to different implementations of the advection scheme and surface parametrization. It can be confirmed that the main drawback of the Newtonian relaxation method Eq.?? is the decrease of turbulence intensity when the streamwise velocity is assimilated towards the prescribed target wind profile. But in this case with a coarse grid the returns to the state of the upstream flow. Results for the simulations in N1 averaged over the last 20 min. Vertical profiles of the streamwise mean velocities in a) and b) and the streamwise in c) and d) for different relaxation times τ inside the nudging area (2.5-3.5 km, left column) and downstream of the nudging area (4-5 km, right column). The black solid line shows the quantities for the upstream zone from 0-2 km. The gray dotted line in a) and b) presents the target wind profile. The red (gray, orange) line refers to the relaxation times $\tau = 30$ s ($\tau = 60$ s, $\tau = 300$ s). The black thin dashed line in c) and d) shows the reference from the ESDU 85020 data for a smooth surface. 3d). Sensitivity studies reveal that a longer relaxation time than the 30 s used here leads to smaller turbulence damping but to a poorer adjustment to the target velocity profile (not shown). This result is in agreement with previous findings by Neggers et al. (2012).

3.1 Results of the Assimilation Method using the Vibration Equation

460

465

490

470 The assimilation method using the vibration equation was implemented in EULAG and tested for different angular frequencies $\omega_0 = 2\pi f_0$ in order to investigate the influence of the method on the flow calculated in EULAG and to validate it with the results of Nakayama and Takemi (2020). They mentioned that f_0 must have a value smaller than the frequency of the peak in the energy spectrum in order to prevent damping of the turbulent fluctuations. Figure ?? a) and b) shows the time-averaged streamwise mean wind velocities for different values of the frequency f_0 . Inside the nudging area the mean velocity is well adjusted to the target wind profile for all tested frequencies. With the Newtonian relaxation represented by Eq. 6 instead, the TKE is 2.5 to 3 475 times higher when compared to the upstream values (Fig. 3 e). From this result it is concluded that TKE is not damped if the applied forcing of the assimilation method acts on the mean flow field $\langle v \rangle$ in Eq. 6, not on the local velocity values at each grid point as in Eq. 4. The TKE is also larger than upstream when the vibration method is used (Fig.??a). Behind the nudging zone a small tendency towards the original wind profile can be found for all three cases (Fig. ??b). This effect can be seen as well in Fig. 8 in Nakayama and Takemi (2020). A difference is that in the with EULAG the mean velocities are nudged better towards the target profile for smaller frequencies. For $f_0 = 0.005$ 3 f) with values up to two times higher. In particular, above z = 150 m the increase in TKE is not as large in V1 (max. $0.18 \text{ m}^2 \text{ s}^{-1}$ at z = 100 mand x = 3 km the offset of the mean velocity to the target value is about 1 m s⁻²) when compared to <N1> (max. 0.25 m² s⁺² in Fig. 8 in Nakayama and Takemi (2020) while the velocity is fully nudged to the target value in EULAG (Fig. ??a). Regarding the streamwise in Fig. ??c a small increase can be seen in the lower 200 m inside the nudging area. Apparently, a smaller frequency).

In summary, our numerical results are in agreement with those of Nakayama and Takemi (2020). EULAG successfully reproduces the assimilation of the zonal velocity component towards the target profile with all three tested methods. Concerning the TKE profiles, the local Newtonian relaxation according to Eq. 4 leads to a higher increase of the . Further downstream from x=4-5 km the turbulence intensity is still slightly augmented but follows in general the curve of the upstream atmospheric flow. The is again set in relation to data of Engineering Science Data Unit (ESDU)85020 for a smooth surface. In the reference

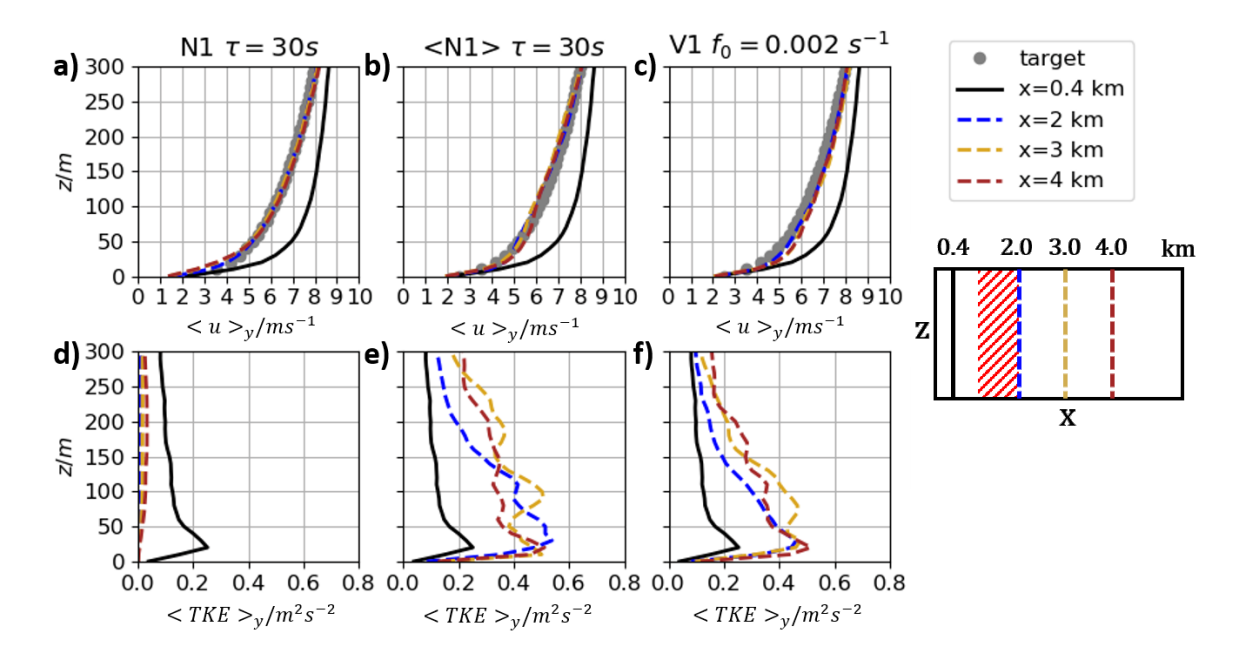


Figure 3. Results for the simulations N1, Eq. 4 and <N1>, Eq. 6 with $\tau = 30$ s and V1, Eq. 7 with $f_0 = 0.002$ s⁻¹. Vertical profiles of the zonal velocities $< u>_y$ in a), b) and c) and the $< TKE>_y$ in d), e) and f) for different downstream positions. The black solid lines show the quantities for the upstream flow at x = 0.4 km. The gray dotted lines represent the target wind profile. The blue (gold, brown) lines refer the downstream positions x = 2 km (x = 3 km, x = 4 km). The scheme on the right side indicates the downstream positions for the evaluation (the red hatched area refers to the nudging zone).

case from Fig. 9 in Nakayama and Takemi (2020) the is a little bit smaller near to the ground and higher above 150 m. The deviation near the ground results from the different modelling of the surface while in the upper layers of the atmosphere the is already higher in the precursor simulation of the reference case. Concerning the Reynolds stress u'w' (Fig. ??e) there is also a little elevation inside the nudging zone which continues further downstream (Fig. ??f). In general it can be stated that for the tested frequencies the turbulent motions are maintained throughout the computational domain and the equilibrium state is not disturbed. Results for the simulations in V1 averaged over the last 20 min. Vertical profiles of the streamwise mean velocities in a) b), the streamwise in c) d) and the Reynolds stress in e) f) for different frequencies f_0 inside the nudging area (2.5-3.5 km, left column) and behind the nudging area (4-5 km, right column). The black solid line shows in all graphs the quantities for the upstream zone from 0-2 km. The gray dotted line in a) and b) shows the target wind profile. The blue (green, red) lines refer to the results for the frequency $f_0 = 0.002$ s⁻¹ ($f_0 = 0.005$ s⁻¹, $f_0 = 0.01$ s⁻¹). The dashed dotted line shows the reference case for $f_0 = 0.005$ s⁻¹ from Nakayama and Takemi (2020). The black thin dashed line in e) and d) shows the reference from the ESDU 85020 data for a smooth surface, destruction of TKE while the simulated resolved turbulence is increased for the Newtonian relaxation and the vibration method at all positions downstream of the nudging zone (when compared to the inflow TKE). Our results for the Newtonian relaxation method are comparable to the results of Allaerts et al. (2020, 2023), while our

495

500

results using the vibration method are in agreement with those of Nakayama and Takemi (2020). Both methods increase the TKE in the simulated neutral case.

Despite the close agreement with Nakayama and Takemi (2020), there are differences in the flow fields downstream when implementing the Coriolis force, as they do in their setup. Without Coriolis forces, a restoring of the flow behind the assimilation region to the initial profile does not occur in our simulations, whereas it does in Nakayama and Takemi (2020). One possible reason could be their inclusion of the Coriolis force. When the Coriolis force was included in our EULAG simulations, the flow evolved temporally beyond the nudging zone away from the target profile as the Coriolis forces are applied to velocity perturbations, which are large beyond the nudging zone (Eq. 2).

4 Results: Data Assimilation within high-highly resolved idealized Simulations

For wind energy purposes, LESs need with a higher resolution in order to calculate the forcing than that used in Sect. 3 must be performed to accurately calculate the interaction of the rotor blades on with the flow. The assimilation methods have been tested and validated in the previous section for a coarse grid of dx = dy = 40 m and dz = 10 m (N1 and V1 in Fig. 2). Now the methods shall Hence, the implemented assimilation methods need to be tested for the high higher resolved simulations with a grid-spacing of dx = dy = dz = 5dx = dy = dz = 5 m (N2 and V2 in Fig. 2), which is i.e. with grid sizes that are commonly used in wind-turbine LESs (cf. Vollmer et al. (2016), Englberger and Dörnbrack (2018), Chanprasert et al. (2022)

1. (e.g., Vollmer et al., 2016; Englberger and Dörnbrack, 2018; Chanprasert et al., 2022). In this section, we extend the work of Nakayama and Takemi (2020) and investigate the assimilation methods on a finer resolved grid.

4.1 Newtonian Assimilation

510

525

530

535

First, we consider the Newtonian assimilation method and quantify the differences between the simulations N1-with coarse grid and N2 with finer grid. In Fig. ?? a)and b) the time-averaged mean streamwise velocity profiles are shown. Inside the nudging area the mean velocity for a forcing with a small relaxation time $\tau = 30$ s is nudged even closer to the target profile in comparison to the simulation N1 (Fig.??a). For the higher relaxation time there are no significant changes. The results for the relaxation time $\tau = 60$ s lie in between the curves for $\tau = 30$ s and $\tau = 300$ s and are not considered in the following. Apparently, with the Newtonian relaxation method the velocity can be nudged even better Figure 4 a)-f) shows vertical profiles of zonal velocities and TKE at different downstream positions for all three tested assimilation methods. This figure is directly comparable to the results of the corresponding coarse resolution simulations shown in Fig. 3. Figure 4 g)-i) present in addition the spectral energy distribution S(k) as function of the wave number $k = 1/\ell(x)$, where $\ell(x)$ is the length ranging from 2 dx to 500 m. The horizontal power spectra at z = 90 m are averaged over the y-direction and are presented for the flow upstream, inside and downstream of the nudging zone.

Starting with the local Newtonian relaxation, the zonal velocity is assimilated precisely towards the target profile on the fine grid than on the coarse grid. Results for the simulations in N2 with Newtonian assimilation technique and fine grid resolution averaged over the last 20 min. Vertical profiles of the streamwise mean velocities in a) b) and the streamwise in c) d) inside the

nudging area (1.0-1.5 km, left column) and behind the nudging area (2.0-2.5 km, right column). The black solid line shows in all graphs the quantities for the upstream zone from 0-0.5 km. The gray dotted line in a) and b) shows the target wind profile. The brown (orange) lines refer to the results for the simulations with $\tau = 30 \text{ s}$ ($\tau = 300 \text{ s}$). The black thin dashed line in c) and d) shows the reference from the ESDU 85020 data for a smooth surface. Regarding the streamwise s in Fig. ?? c) and d) it can be seen that the intensity is more strongly diminished in the nudging zone for $\tau = 30$ s than in the case with coarse grid and only 15% at 200 m is preserved. In the case with a larger relaxation time there is only little decrease of the similar to the simulation N1 for simulation N2 (Eq. 4) and does not change after the relaxation zone at x = 3 km or x = 4 km (Fig. ??e and d). While the intensity recovered in the simulation N1 downstream of the nudging area this is not the easefor N2. Only in the lower layers of the atmosphere up to a height of z = 60 mthe intensity level of the upstream flow is reached. At z = 200 m only 40% of the upstream is preserved. Compared to the coarse grid the turbulence intensity couldn't be recovered to the same extent in the fine grid. With the fine grid spacing which is necessary for wind-turbine wake simulations it is therefore crucial that the impact of the nudging method on the turbulence intensity is limited to a minimum. Once turbulence is destroyed in the atmosphere it can't be recovered to the same extent because only near-surface shear can produce turbulence in the neutral boundary layer. 4 a). For this case, however, the TKE is decreased to values below 0.05 m² s⁻² inside the nudging zone and further downstream. From this result, we deduce that the effect of local Newtonian relaxation on small-scale turbulence is not resolution dependent, since this is the same finding as in the corresponding coarse resolution simulation N1.

4.1 Vibration Assimilation

Similarly,

540

545

550

555

560

565

In contrast, when the Newtonian relaxation is applied in simulation <N2> (Eq. 6), the simulations with a refined grid are conducted with application of the assimilation technique using the vibration equation (cf.V2 in Fig. 2). The analysis of the time-averaged streamwise mean velocity, the and the Reynolds stress u'w' is shown in Fig. ??. The results $f_0 = 0.005 \text{ s}^{-1}$ lie in between the curves for $f_0 = 0.002$ target velocity profile is underestimated by 0.8 m s^{-1} and $f_0 = 0.01 \text{ s}^{-1}$ are not taken into account for the following considerations. For all frequencies the mean velocity is well adapted to at x = 2 km and z = 50 m. At higher altitudes, the x = 2 km profile is consistent with the target profile (Fig.??a). Downstream of the nudging area the velocity increases in both cases in the lower part of the atmosphere near the surface but still matches well with the target velocity profile 4 b). Further downstream, at x = 3 km and x = 4 km, the velocity fluctuates slightly around the target profile. This issue is probably due to the rather large TKE, which is 2-3 times higher downstream than in the upstream flow (Fig. 4 e). The Newtonian relaxation to the target profile in simulation <N2> (Fig.??b) . Regarding the streamwise 4 b) is slightly worse than in simulation <N1> (Fig.??e)a decrease of the can be seen in the nudging zone for both cases above z = 100 m which is stronger for the higher frequency. Beneath z = 100 m the is slightly increased for $f_0 = 0.002 \text{ s}^{-1}$ and remains close to the original for the higher frequency. Behind the nudging domain (Fig. ??d) the is similar to the original profile below z = 100 m in both cases and recovers slightly above z = 100 m for $f_0 = 0.002 \text{ s}^{-1}$. For the higher frequency of $f_0 = 0.01 \text{ s}^{-1}$ the did not recover, it even diminishes further down to 40% at z = 200 m 3 b), and the TKE is affected in the same way (Fig. 3 e and 4 e),

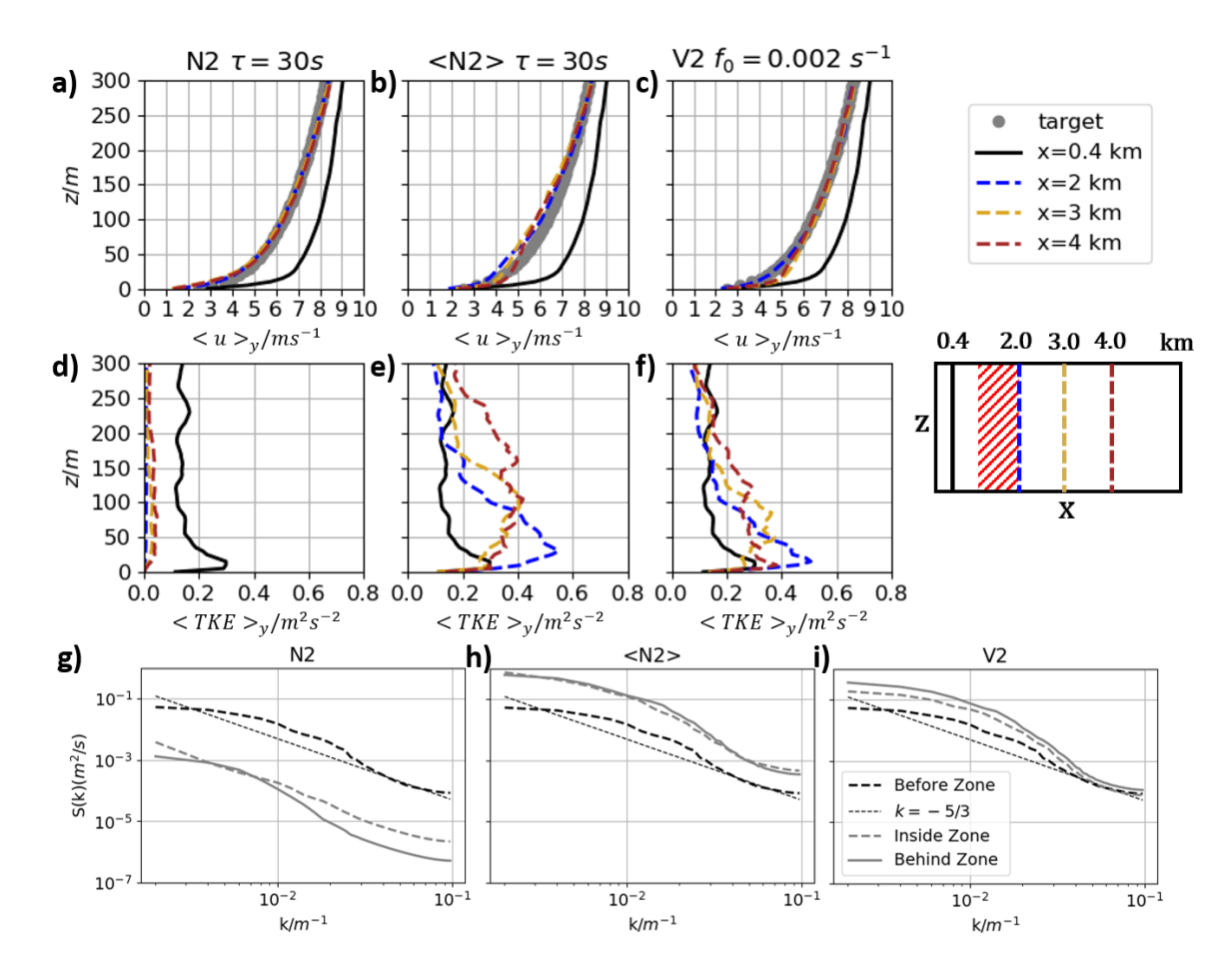


Figure 4. Results for the simulations with Newtonian relaxation N2 (Eq. 4, $\tau = 30$ s) and <N2> (Eq. 6, $\tau = 30$ s) and the vibration method V2 (Eq. 7, $f_0 = 0.002$ s⁻¹) with the fine-grid resolution. Vertical profiles of the zonal velocities $\langle u \rangle_y$ in a), b) and c) and the $\langle TKE \rangle_y$ in d), e), f). The black solid lines show the quantities for the upstream flow at x = 0.4 km. The gray dotted lines show the target wind profile. The blue (gold, brown) lines refer to the results for x = 2 km (x = 3 km, x = 4 km). The scheme on the right side indicates the downstream positions for the evaluation. In g), h) and i) the horizontal spectra (z = 90 m, length 500 m, width 3000 m) for each simulation is shown for the flow before (black dashed), inside (gray dashed) and downstream (gray solid) of the nudging zone.

which means that there is no dependence on the resolution when using the Newtonian relaxation as an assimilation method for the LES.

To gain a more detailed insight into the effects of the forcings applied in the simulations N2 (Eq. 4) and <N2> (Eq. 6) on the flow field, lateral cross-sections of instantaneous u and v-fields are presented in Fig. 5(a-l). The inflow fields at x = 500 m are the same for the two simulations shown in Fig. 5 (a, g) and they basically represent the flow field of the precursor simulation P2. In the relaxation region, however, there is a striking difference between these both Newtonian relaxation methods (Fig. It can be concluded that ahigher frequency in the assimilation method suppresses the more than a smaller frequency. This is in

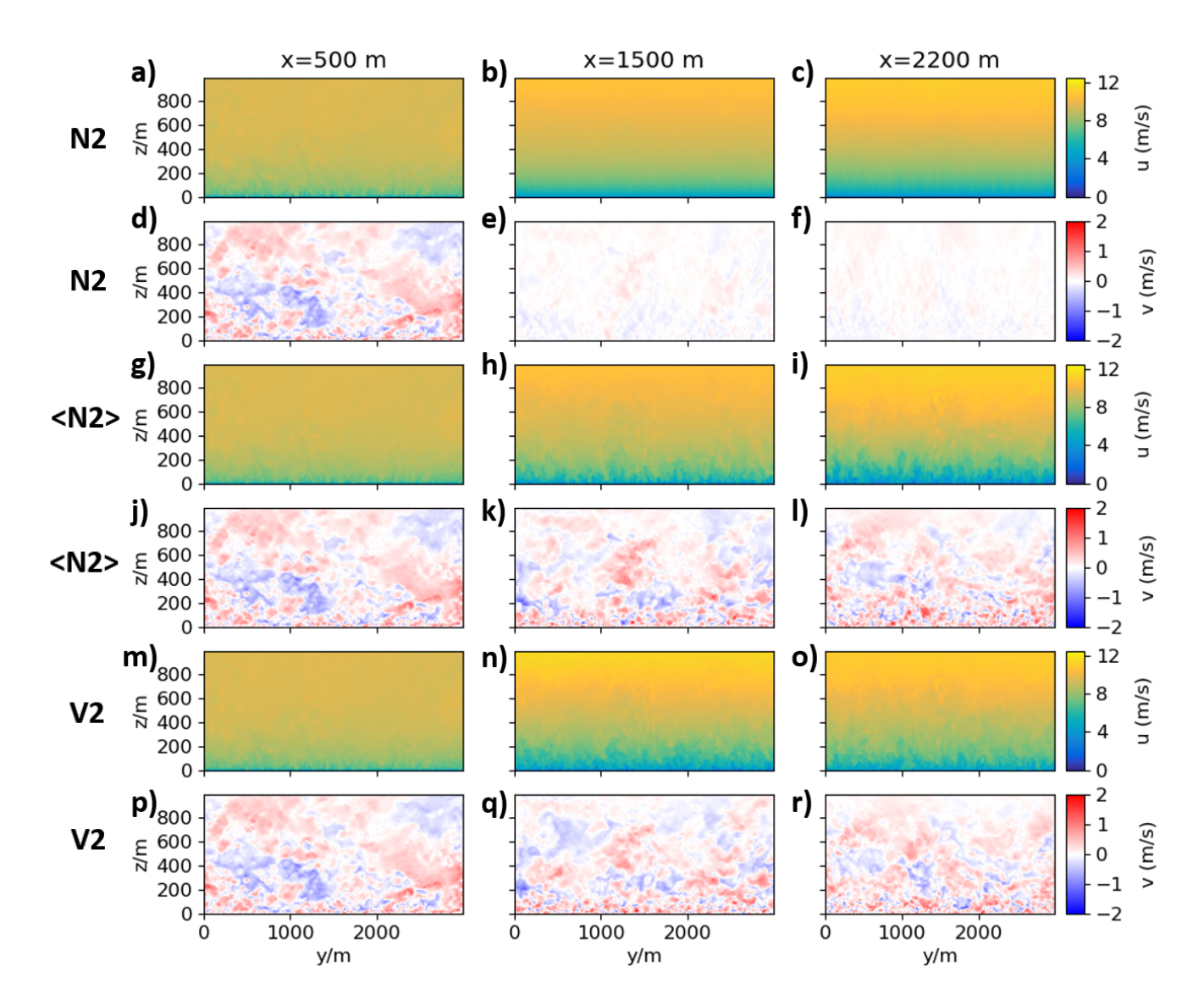


Figure 5. Vertical cross sections of the zonal and the meridional velocity u and v for x = 500 m upstream, x = 1500 m inside and x = 2200 m downstream of the nudging zone. The results are shown for the simulations N2 (a-f), <N2> (g-l) and V2 (m-r).

agreement with the findings of Nakayama and Takemi (2020) (cf. Fig.9). The mean velocity is adjusted accurately 5, b, h). While in both cases the absolute value of the u-field is adjusted to the target profile for both frequencies. Compared to the simulations with a coarse grid V1 by a deceleration of the mean flow, the flow field in simulation <N2> (Fig. ??e and d) the is diminished and not increased. Concerning the Reynolds stress u'w' in Fig. ??f an increase of max. 90% 5 h) is still turbulent and no laminarization occurs, as it is the case in the simulation N2 (Fig. 5 b).

580

The same difference can be observed at z = 50 m behind the nudging zone compared to 100% at z = 60 m in Fig.??f. At z = 200 m there is a max, decrease of 50% in Fig. ??f and an increase of 76% in Fig. ??f. Turbulent fluctuations are damped more in higher layers of the atmosphere in the simulations with the fine grid. It can be concluded that the performance of the assimilation method with the vibration equation is more suitable for the finer grid spacing. When a target profile is assimilated with the Newtonian relaxation method a substantial decrease of the must be accepted. Indeed, the assimilation methods have a different impact on the atmospheric flow when the grid spacing is finer. While the mean velocity can be assimilated to the same extent, the is more effectively reduced for the simulations with finer spacing. This effect can be reduced when the assimilation method with the vibration equation is used. With $f_0 = 0.002$ s⁻¹ the is decreased but is still in the proximity of the ESDU reference profile. Consequently, it is recommended for wind-turbine simulations to work with the assimilation technique using the vibration equation following Nakayama and Takemi (2020) because of the smaller impact on the atmospheric turbulence. Results for the simulations in V2 with the vibration assimilation method and fine grid resolution averaged over the last 20 min. Vertical profiles of the streamwise mean velocities in a) b), the streamwise in c) d) and the Reynolds stress in e) f) for different frequencies f_0 inside the nudging area (1.0-1.5 km, left column) and behind the nudging area (2.0-2.5 km, right column). The black solid line shows in all graphs the quantities for the upstream zone from 0.0-0.5 km. The gray dotted line in a) and b) shows the target wind profile. The blue (red) lines refer to the results for the frequency $f_0 = 0.002 \text{ s}^{-1}$ ($f_0 = 0.01 \text{ s}^{-1}$). The black thin dashed line in c) and d) shows the reference from the ESDU 85020 data for a smooth surface, v-components (Fig. 5, e, k). The turbulent fluctuations of v around its mean of zero are preserved within the relaxation region in simulation <N2> (Fig. 5 k), while they are strongly suppressed in simulation N2 (Fig. 5 e). This behaviour in the relaxation region at x = 1500 m, which continues downstream (x = 2200 m), explains the nearly perfect adjustment of the vertical profile in simulation N2 (Fig. 4 a). In contrast, the small deviations of the mean u-profile that occur in simulation <N2> are an effect of preserving the turbulence characteristics. The conclusion is that the vertical profile of the flow velocities is not meaningful on its own, but that the behavior of the TKE is decisive.

5 Assimilation towards a measured Wind Profile in Krummendeich

585

590

595

600

a) Comparison of the time-averaged mean velocities \$\overline{u}\$ and \$\overline{v}\$ of the precursor simulation for the , the measurements and the target velocity profiles extracted from . The black (pink) solid line refers to the mean streamwise (spanwise) velocity in the precursor simulation while the black (pink) dashed line shows the streamwise (spanwise) target profile. The light blue (dark blue) line presents the observations for the streamwise (spanwise) velocity with the . b) Temperature profile measured with the microwave radiometer (black dashed line) in comparison with the dry (red line) and moist (green line) adiabatic lapse
rate. In this part of the study the target profile is near to a measured velocity profile for the wind-farm site at Krummendeich. observations and data from a microwave radiometer have been analysed in order to search for a situation similar to a near the ground. As period was chosen the 19.11.2021 18 UTC to 19 UTC which features strong wind shear near to the ground and a larger wind veer in the boundary layer. As continuous measurements are only available from \$z = 60\$ m up to \$z = 470\$ m a simulation with was conducted for this period and continuous streamwise and spanwise velocity profiles were extracted. The

setup and the extraction of the used target profiles is described in appendix A. Figure??a shows the velocity profiles of and for the idealized neutral precursor simulation. The above finding is supported by analysing the spectra (Fig. 4 g-h). In the case of the local Newtonian relaxation in simulation N2, the spectral energy density before the nudging (in P2in comparison to the independent measured velocities and the target wind profiles which were extracted from . A substantial difference is seen in the meridional mean velocities in the precursor simulation for the the meridional component of the velocity is nearly zero over the whole height, while the target profile shows positive values beneath z = 200 mand negative velocities above until - 7 m) is much higher. This local Newtonian relaxation basically reduces the energy on all scales in the whole domain, resulting in a strongly reduced value of S(k) to less than 10% of the inflow energy in Fig. 4 g) in comparison to Fig. s4 h) in simulation <N2>. Applying the Newtonian relaxation in simulation <N2>, the spectral energy density increases on all scales. This finding is in agreement with the increase in the resolved TKE (Fig. 4 e).

In the following, the application of the vibration method and the comparison of the corresponding simulation V2 with the simulation <N2> of the Newtonian relaxation is presented in order to investigate the difference of these two different methods on a fine grid. The vertical profile of the zonal velocity results in an exact adjustment to the target profile at x = 2 km (Fig. 4 c). Only at z = 20 m the actual velocity component is slightly overestimated compared to the target profile at x = 3 km and x = 4 km. At all other heights, the simulated velocities overlap nearly perfectly with the target profile. Figure 4 f) shows the vertical profiles of TKE. The TKE at the downstream positions is 1.5-2 times higher than in the upstream flow beneath z = 150 m. Above z = 150 m, there is only a small deviation between the downstream and upstream TKE (± 0.06 m² s + 2 at z = 600 m. Figure ??b shows the temperature profile in).

The vibration method leads to a more precise assimilation towards the target profile in the fine-grid case of simulation V2 in comparison to the dry and moist adiabatic lapse rate. In the lowest 350 m the temperature profile shows a neutral stratification because the lapse rate is close to the moist adiabatic lapse rate (cf.Rohli and Li (2021)). This was the defined requirement for the selection of this atmospheric situation. However, the graph shows that the atmosphere is stably stratified above 350 m because the lapse rate is smaller than the reference lapse rate. Hence, we will first apply the assimilation method to the idealized P2 (cf.Sect. 2.4) in Sect. ?? and afterwards to an idealized (cf.P3 in Sect. 2.4) in Sect. ?? coarse-grid simulation V1 (compare Fig. 3 c and 4 c). Furthermore, the impact of the vibration method on the TKE is less pronounced for the fine-grid simulation (Fig. 4 f) than in the coarse-grid simulation (Fig. 3 f), suggesting that the vibration method performs better with higher resolution.

4.1 Neutral Boundary Laver as Precursor Simulation

640

645

As the temperature profile The impact of the different forcings f in Eq. 2 due to the Newtonian relaxation (Eq. 6) and due to the vibration method (Eq. 7) on the instantaneous flow field is presented in Fig. 2. shows a neutral stratification beneath 350 m we use in a first approach the idealized P2 described in section 2.4 as precursor simulation for 5 m)-r) for both u and v components of simulations <N2> and V2. In general, the turbulent structure is very similar in both simulations. This could be interpreted that both assimilation methods basically impact the horizontal mean (Fig. 4 b+c) and, consequently, the resolved TKE (Fig. 4 e+f). However, the turbulent 3 D flow structure in Fig. 5 (i, 1, 0, r) is only affected to a small extent. The increase

of turbulence - especially below 150 m height - within and after the nudging zone compared to the region in front (Fig. 4 e-f) is partly due to an increase of $\frac{\Delta u}{\Delta x}$ in the assimilation to the realistic wind profile. Here the results for the fine grid are shown with dx=dy=dz=5 m. While the offset of the space-averaged mean velocity of the precursor simulation \overline{u}^P (averaged over the whole domain) to the mean of the target profile (averaged over the height of the) \overline{u}^T is large,

$$\overline{u}^P >> \overline{u}^T \quad or \quad \overline{u}^P << \overline{u}^T,$$

the velocity at each grid point has to be changed:

$$u_{i,j,k}^{new}(z) = \alpha \overline{u}^p(z) + u_{i,j,k}^{\prime p}$$

with-

650

655

660

665

670

$$\alpha = \frac{\overline{u}^T}{\overline{u}^P} \quad .$$

Here, $u_{i,j,k}^{new}$ is the new velocity value of the inflow field at every grid point, $\overline{u}^p(z)$ is the space averaged mean value at every height of the precursor simulation and $u_{i,j,k}^{\prime p} = u_{i,j,k}^p - \overline{u}^p(z)$ is the fluctuation at every grid point i,j,k of the precursor simulation. This was not necessary for the investigations with the idealized profiles in Sect. 3 and Sect. 4, in comparison to the inflow profile of P2. It is also partly an effect of the Newtonian relaxation itself, as the mean velocity of precursor simulation and target profile was similar. We successfully tested the assimilation method for target profiles with $\alpha = 0.67$ until $\alpha = 2$. The amplitude of the velocity fluctuations and, therefore, the is not changed by this adaption. For the zonal velocity profile on 19.11.2021 extracted from the value $\alpha = 1.44$. Here two different simulations (I) and (II) are shown. In the first one (I), v-contribution to the TKE is also larger in simulation <N2> in comparison to simulation V2, whereas $\overline{v} = 0$ in both cases (not shown).

For a more detailed comparison between the Newtonian and the vibration approach, the spectral energy density is shown in Fig. 4 h)-i) for simulations <N2> and V2. On large scales (small wave number k), the target velocity values are reduced (blue eurves spectral power S(k) increases similarly behind the nudging zone. In the nudging zone, however, the vibration method does not instantaneously reach the final spectral energy density behind the nudging zone. The transition occurs not as abruptly as in simulation <N2>. This abrupt transition could be an effect of the Newtonian relaxation itself applied in <N2>, which also is responsible for the higher TKE in Fig.??):

$$u(z)_{new}^T = \frac{1}{\alpha} u(z)^T$$
 with $\alpha = 1.44$.

The second (II) was computed with the original target profile and an adapted inflow field following Eq. 8 (red curves in Fig. 75). The frequency in the vibration assimilation method was set to $f_0 = 0.002$ s 4 e) in comparison to Fig. 4 f). Further, going to smaller scales (larger wave number k), the impact of the vibration method on the energy spectra decreases and for k > 0.04 m⁻¹ as the previous investigations showed that this value gives the best results. The vibration assimilation method was able to nudge the streamwise velocity towards the target wind profile in both cases. In the lowest 50 man increase of 0.4 - 0.6 m s⁻¹ an equal

energy level can be seenbehind the nudging area from 2.0-2.5 km as well as a small underestimation of 0.2-0.5 m s⁻¹ between z = 300 m and z = 500 m (Fig. ??a). Regarding the mean spanwise velocity it was not possible to nudge towards the strong negative values because the Courant-Friedrich-Lewy-criterion was violated during computation. We kept the original profile up to a height of z = 200 m as wind turbines usually operate in . This is also different in comparison to the behaviour of simulation <N2>.

680

685

690

695

700

705

710

All methods tested assimilate the mean flow to the lowest layer of the atmosphere. Above z = 200 m the spanwise velocity of the target profile in Fig. ??a has been reduced to the profile in Fig. ??b. Inside the nudging zone there is an exact assimilation towards the target profile with an offset less than 5% in the WT region and a slightly larger offset of 10% above 600m. Downstream of the nudging area the velocity strongly tends to the upstream state above z = 200 m(Fig. ??b). For the simulation (II) the spanwise mean velocity continues to be overestimated behind the nudging zone below 200 m. The streamwise's show an increase in both cases below z = 100 m and a decrease above (Fig. ??c). In the nudging area at z = 200 m only 45% of the is preserved in case (II) and 60% in case (I). Downstream of the nudging area the streamwise recovers and reaches even higher values than in the precursor simulation. The spanwise increases in both cases up to a height of z = 300 m and does not change considerably regarding the nudging zone and the flow behind the area (Fig. ??d). At z = 100 m the spanwise is doubled for the simulation (II) reasonably well. The local Newtonian relaxation method applied in N1 and 2.5 times larger for (I). Due to stronger wind shear and wind veer in the target profiles the equilibrium state of the precursor simulation is changed and more turbulent kinetic energy is generated. This is the reason why an increase in the can be seen especially behind the nudging area. A disadvantage of the assimilation of the velocity in this idealized towards the measured streamwise and spanwise velocity profiles is the strong wind veer in the target profile which does not occur in the idealized case. Apparently it is not sufficient to consider only the lowest 350 m where the temperature profile is near to the moist adiabatic lapse rate and the atmosphere is neutrally stratified (cf. N2 is not applicable for wind-turbine applications, as the TKE of the assimilated flow fields becomes too small and flow itself too smooth. It is clear that in both the vibration method and the Newtonian relaxation method, turbulence still persists after assimilation to a given target velocity profile, in comparison to the local Newtonian approach, in which a laminarization occurs. In both assimilation methods the flow is more turbulent than the inflow profile, meaning that both methods add additional turbulence. Including the spectral analysis, the integral approach of the vibration method leads to a more gentle adjustment of the energy content, while the wind profiles adjust similarly well in both approaches. The resolution impact in case of the Newtonian relaxation methods is only weakly pronounced, while the vibration method shows improved results for an increased resolution. Despite these minor differences, these two methods are suitable for wind-energy applications with grid spacings of up to 5 m.

The coarse and fine resolution results show a very similar behaviour of the resulting flow field for using the Newtonian and the vibration approach. The following simulations, which perform an assimilation to observed profiles from the WiValdi wind park, are conducted by using the vibration method only, as, to our knowledge, this method has not been previously tested for wind-turbine relevant resolutions. For a detailed investigation of the Newtonian approach for wind-energy applications and modifications of the approach itself we refer to Allaerts et al. (2020, 2023). They also investigated the vibration method,

but only in combination with the Newtonian approach, with no significant difference in the behaviour of their algorithm (Allaerts et al., 2020).

715 5 Results: Assimilation towards a measured Wind Profile at the wind-farm site WiValdi

In this section, the continuous wind profile from the WRF simulation (Appendix A) is used as target profile for the data assimilation. As mentioned above in Section 2.3, this profile is close to a measured velocity profile from the wind-farm site WiValdi (Fig. 1). The objective of the simulation SO (cf. Fig. 2) is the generation of a more realistic inflow field for a wind-turbine simulation which will be discussed in Section 6.

The data assimilation is now more complex, as both the zonal and the meridional components have to be adjusted to the target profiles. This extends the work of the previous chapter where the assimilation was only applied to the zonal velocity component. Hence, the simulation SO is a step towards more realistic inflow fields guided by observational data. As described above, the vibration method is used in the following for the adjustment towards the WiValdi profile.

In a first approach (not shown), we tested if the velocities of the neutral precursor simulation P2 could be assimilated towards the target profiles \overline{u}_{WRE} and \overline{v}_{WRE} from Fig. P2b). As the temperature profile shows a stably stratified configuration above 350 mwe will use in the next section a stably stratified precursor simulation. Results for VO of the assimilation towards measured velocity profiles with the as precursor simulation and application of the vibration assimilation method averaged over the last 20 min of the simulations. The blue profiles show the results for (I) and the red profiles for (II), a) mean streamwise velocity b) mean spanwise velocity c) streamwise d) spanwise. The black solid lines refer to the upstream velocities in a) and b) and s in c) and d) for x = 0 - 0.5 km. The black dashed line in a) represents the adapted inflow field for (II). The gray dotted line in a) (b) refers to the streamwise (spanwise) target velocity profile. The colored solid (dashed) lines show the values for the frequency $f_0 = 0.002$ s⁻¹ inside (behind) the nudging area from x = 1.0 - 1.5 km (x = 2.0 - 2.5 km). The black thin dashed line in c) shows the reference from the ESDU 85020 data for a smooth surface. 1. However, the meridional velocity component in P2 is close to zero over the whole boundary layer height, while the target profile has positive values below z = 200 m and decreases above until -7 m s⁻¹ at z = 600 m. This strong veer of the flow in the target profile contrasts the pure zonal flow in P2. The assimilation of the flow in P2 towards the new target profile created numerical artefacts.

5.1 Stable Boundary Laver as Precursor Simulation

725

730

735

740

As response to the limitations of the results in the previous section, we propose to use a precursor simulation of a computed by For this reason, we use another precursor simulation P3 of a stable boundary layer of Englberger and Dörnbrack (2018) which has similar \overline{u} - and \overline{v} -profiles compared to the target profiles. In this configuration wind shear andespecially wind veer are present in the atmospheric flow. Figure ?? shows been introduced in Section 2.4. Wind shear and, in particular, wind veer both occur in this boundary layer flow. The magnitude of the inflow field for the simulation with data assimilation has been modified according to Eq. 8 with $\alpha = 1.25$ ($\alpha = 0.4$) for the zonal (meridional) velocity components. Figure 6 a)-b) show the mean velocities \overline{u} and \overline{v} of the $< u >_v$ and $< v >_v$ of the modified precursor simulation for the SBL in comparison to

the target velocity profile. Comparison of the time-averaged mean velocities and of the precursor simulation for the and the target velocity profiles. The black (gray) solid line refers to the mean streamwise (spanwise) velocity in the precursor simulation while the black (gray) dashed line shows the streamwise (spanwise) target profile. We expect a better performance of the assimilation method as wind veer and shear are present in the precursor simulation P3 too. In this simulation the nudging zone ranges from x = 2.0 - 3.0 km. The assimilated profiles for the streamwise and the spanwise mean velocity can be seen in Fig. profiles. The results for the assimilated velocities and the TKE are shown in Fig. 6 for the outflow of the nudging zone and the position 200 m downstream of the nudging zone. The wind turbine for the simulation presented in section 6 is placed at this position.

With a frequency of $f_0 = 0.002 \,\mathrm{s}^{-1}$ in the vibration method a precise assimilation towards the target zonal profile is achieved above z = 100 m (Fig. 6a) and b). The streamwise mean velocity has been adapted for the initialization field and the inflow velocity field according to Eq. 8. There is a very good match for \overline{u} already inside the nudging area and the wind speed adjusts even more further downstream. The assimilated profile for the spanwise velocity component follows the target wind profile very well. Only between 30. Beneath z = 100 m, the zonal wind component is underestimated by up to 1 m s⁻¹. but it is very close to the target profile at the position of the wind turbine. Figure 6 b) shows that the meridional velocity component can be adapted to the target profile with a slight underestimation (overestimation) of less than 0.3 m s^{-1} between z = 50 m and 125 m the velocity is slightly underestimated behind the nudging area. Hence, the vibration assimilation method is capable to assimilate the streamwise and spanwise mean velocity towards the target profiles. Compared to the assimilation in the (Fig.??) notably the spanwise velocity could be nudged towards the target profile and did not tend back to the spanwise profile of P3 downstream of the nudging zone. Results for SO of the assimilation towards the measured boundary layer profile with a as precursor simulation and application of the vibration assimilation method averaged over the last 20 min of the simulation. a) mean streamwise velocity b) mean spanwise velocity c) streamwise d) spanwise. The black solid lines refer to the upstream velocities in a) and b) and s in c) and d) for x = 0 - 2 km. The gray dotted line in a) (b)) refers to the streamwise (spanwise) target velocity profile. The blue solid (dashed) lines show the values for the frequency $f_0 = 0.002 \text{ s}^{-1}$ inside (behind) the nudging area from x = 2.0 - 3.0 km (x = 3.5 - 4.5 km). Regarding the streamwise and spanwise z = 100 m (z = 120 m and z = 250 m).

760

765

Regarding TKE, shown in Fig. 6 c), it can be seen that the turbulent regime is mostly unchanged due to the vibration method at the downstream positions. Over the whole boundary layer height the TKE stays within a range of ±0.01 m² s⁻². The spectral analysis in Fig.6 c) and d) an increase is noticeable. Near to the ground the streamwise inside the nudging zone is over three times higher than in-6 d) shows the spectral energy S(k) at z = 90 m, which is close to hub height of the wind turbine in WiValdi. Similar to the neutral simulation V2, the assimilation increases the spectral energy at large scales. At small scales (large k-values), its comparable behind and in front of the relaxation zone.

A visualization of the u and v-components of the flow for a cross-section before, inside and downstream of the and over five times higher behind the zone. With growing height the decreases and has the same magnitude above z=150 m inside the nudging zone. For x=3.5-4.5 km the is still four times higher at z=100 m and two times higher at z=250 m. The target profile shows a velocity gradient over the whole height while shear is only present up to z=100 m in the precursor

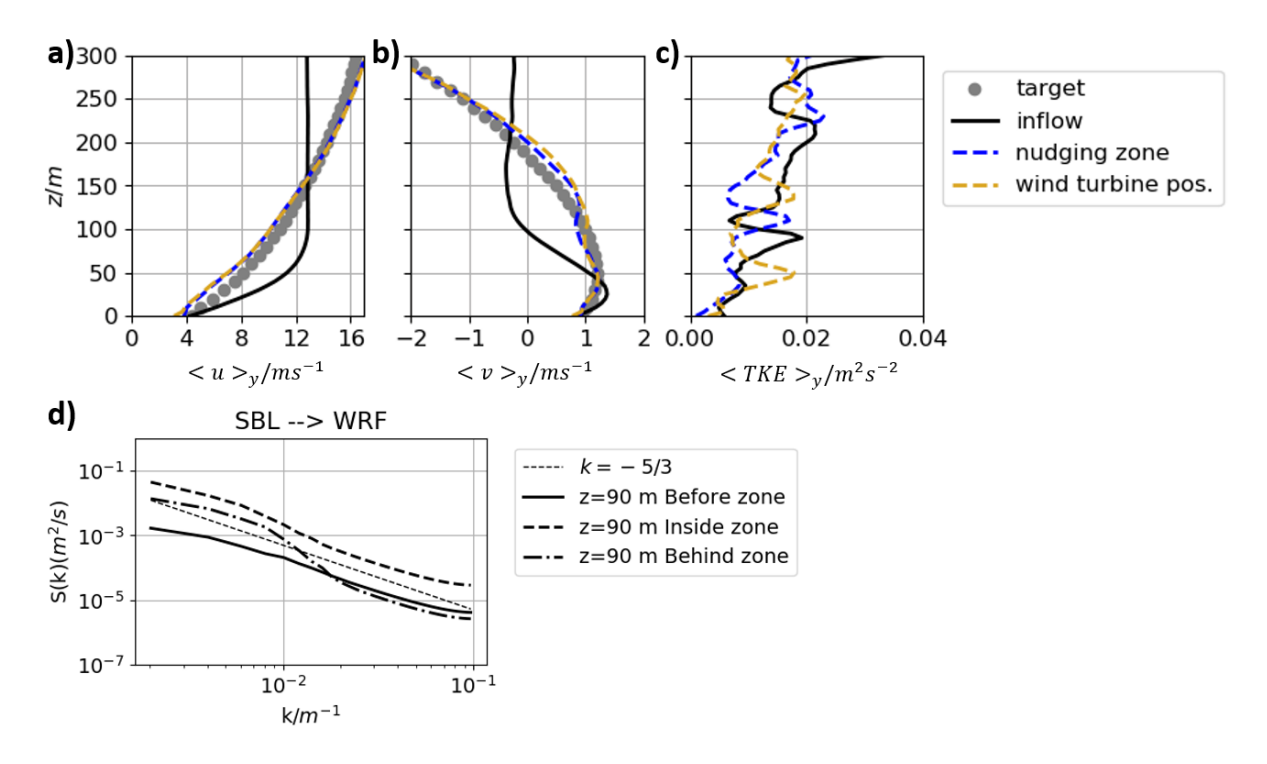


Figure 6. Results for SO of the assimilation towards the representative WRF velocity profile with the precursor simulation P3 and application of the vibration method ($f_0 = 0.002 \, \mathrm{s}^{-1}$), a) zonal velocity $< u >_u b$) meridional velocity $< v >_u c$) $< TKE >_y$. The black solid lines refer to the values upstream of the nudging zone. The gray dotted lines in a) and b) indicate the zonal and meridional target velocity profile. The blue lines show the values for the outflow of the nudging zone while the gold lines indicate the position for the wind turbine in Sect. 6. In d) the horizontal energy spectra is shown for the height $z = 90 \, \mathrm{m}$ (length 500 m, width 3000 m) for the flow before, inside and behind the nudging zone.

780

790

simulation. The increase of the shear beneath z=100 m leads significantly to a higher turbulence intensity. The spanwise is also about three times higher over the whole height compared to the precursor simulation is presented in Fig. 7. In general, the upstream flow (Fig. 7 a and d) is less turbulent compared to the NBL in the previous section (e.g., Fig. 5 a and d), which is a typical characteristic of the SBL, as the only turbulence source is shear close to the surface. The adjustment of the u and v-components is clearly visible for the downstream positions while the turbulent structures are not affected considerably (Fig.6d). In the precursor simulation wind veer occurs only in the lowest 100 m. Above, the spanwise mean velocity \overline{v} is nearly constant at $\overline{v} = -0.2$ m s⁻¹. The assimilation leads to a spanwise velocity profile where veering is present over the whole height which increases the spanwise. Figure ?? gives an overview of 7 b, c, e, f). The zonal flow component is decelerated below 150 m in height and accelerated above. The vibration method lifts the sign-changing height of the meridional velocity component v from 100 m to 200 m. It further increases the gradient at this transition zone, while the 3 D turbulent structure of v is not changed by this process. This pattern prevails also at the wind turbine position, outside of the nudging zone.

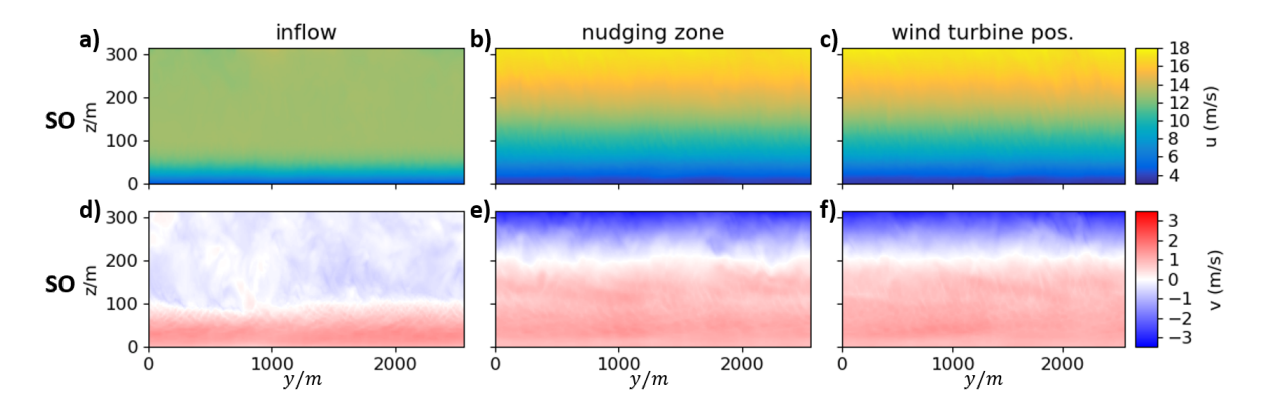


Figure 7. Vertical cross sections of the zonal and the meridional velocity u and v for the inflow area before the nudging zone (a, d), the outflow of the nudging zone (b, e) and downstream of the nudging zone at the wind turbine position (c, f). The results are shown for the simulation SO.

In summary, the results for the considered precursor simulations with the application of the vibration assimilation method. It can be concluded, that the wind profiles of the SBL are better suited for the assimilation towards the measured velocity profiles . Figure ??a and b show a good accord of the velocities could be adjusted efficiently towards the representative WRF velocity profiles using the vibration method. Obviously, a successful data assimilation requires that the target profiles, which prescribe wind shear and veer, are generated by a precursor simulation with similar characteristics. Furthermore, it is interesting that the resolved TKE in the SBL downstream to the nudging zone. Especially the gap between the assimilated spanwise velocity profile for the and the target profile is striking (Fig. ??b). Indeed, the s in Fig. ??c and d for the are closer to the -measurements and the reference data from (resolved) than for the . With the as precursor simulation the s are changed due to the assimilation method to a higher intensity than in the precursor simulation. However, there might be mesoscale effects which are not taken into account by the assimilation method and the precursor simulation. Comparison of the a) mean streamwise velocity b) mean spanwise velocity c) streamwise and d) spanwise for the two different precursor simulations and - and -data averaged over the last 20 min of the simulations. The black (red) lines refer to simulation with a () as precursor simulation. The solid (dashed) line shows the curves upstream (downstream) to the nudging zone. The gray dotted line in a) (b)) refers to the streamwise (spanwise) target velocity profile out of . The light blue line in a) (b)) shows the -data for the streamwise (spanwise) velocity and in c) the streamwise. The dark blue line in e) (d)) shows the streamwise (spanwise) calculated from the flow field, is not considerably changed when using the vibration method for data assimilation, as it is in the neutral case. In the previous Section 4, we have shown that the velocities are not changed further downstream of the nudging zone. The same behavior is observed for the case discussed here. Thus, using the vibration method allows for the inclusion of a wind turbine at a downstream position, after the relaxation occurred. This will be presented in the next section.

795

800

805

6 Results: Analysis of the Wind-Turbine Wake for an assimilated Atmospheric Inflow

In this section the assimilation of a precursor simulation towards the realistic wind profiles shall be combined with the simulation of the wake behind a wind turbine. Therefore, the assimilated of section ?? is considered as the vibration assimilation method showed the best performance regarding mean velocity profiles. Behind the nudging zone the wind turbine simulation SO presented in the previous section is repeated with the integration of a NREL 5 MW wind turbine $(h_{bub} = 90 \text{ m}, D = 126 \text{ m})$, located behind the nudging zone (SOW) (Fig. 2). The wind-turbine rotor is modeled in EULAG according to the parametrization presented in section 2.1 and is located at x = 0.3 - 1.3 km and the rotor is placed 200x = 2200 m, i.e. 200 m behind the nudging zoneat x = 1.5 km. The computational domain for the wake analysis has a length of 3620 m which is sufficient for the investigations until 22D = 2772 m behind the rotor. First, we conducted one simulation. Additionally, a reference simulation SW has been computed with the wind turbine and exposed to the original SBL as a reference case. In a second simulation precursor simulation P3 in order to analyse the differences in the developed wakes. With this implementation and comparison, an efficient testing of different target wind profiles and hence different inflow fields for a wind turbine can be achieved. The applicability of this approach is the inflow of the is assimilated by the vibration assimilation method towards the measured target wind profile from Sect. ??. The wake of the wind turbine is computed for a rotor plane which is at hub height orthogonal to the main wind direction, objective of this section.

The time-averaged streamwise (over the last 20 min of the simulation) zonal velocity component for both cases is shown for three x - y planes covering hub height (z = 90 m) as well as the upper (z = 120 m) and lower rotor half (z = 60 m) of the NREL 5 MW rotor in Fig. 8. The influence of the assimilation method on the mean streamwise zonal velocity is clearly visible at hub height (in Fig. 8 d), e) and in the lower part of the rotor (Fig. 8f). The velocities are inflow velocities in front of the wind turbine are reliably reduced towards the slower target wind profile (cf. Fig. As the rotor plane is turned towards the main wind direction, the influence of the changed wind veer is visible in Fig.8d where 6 a). Furthermore, the wake is slightly deflected southwards because of a negative spanwise velocity. Also in Fig.8f a small deflection of the far wake to the north is seen due to the positive spanwise wind speed below the nacelle. The small asymmetry in the near wake in deflected northwards in the assimilated simulation due to the increased vertical gradient of the meridional velocity over the upper rotor half (cf. Fig.8d (f)can be explained by the negative (positive)spanwise velocity above (beneath)the nacelle and the induced flow due to the rotation of the rotor. Furthermore, the 6 b). In contrast, the wake in the reference simulation is only deflected in the lower part of the rotor (Fig. 8 c) because wind veer only occurs in the lowest 100 m of the boundary layer in P3 (cf. Fig. 6 b black curve). Furthermore, the deflection in the simulation SW is not as pronounced as in SOW, as the meridional wind component is smaller ($v_{SW}(60 \text{ m}) < v_{SOW}(60 \text{ m})$).

The streamwise wake extension is decreased for the case with assimilation. For the reference case a velocity deficit $(VD_{i,j,k} \equiv \frac{\overline{u_{1,j,k}} - \overline{u_{i,j}}}{\overline{u_{1,j,k}}}$ of 10% similar in both cases at z = 60 m and z = 90 m. A reduced wake extension is seen at x = 22D behind the rotor at hub height and at x = 20D the deficit reaches a value of 20% z = 120 m for the assimilated case (Fig.8b 8d). In the simulations with vibration assimilation a deficit of 10% (20%) is seen at x = 20D (x = 14D) at hub height (simulation SOW, the zonal velocity deficit of 10% is reached at x/D = 18 in comparison to x/D = 22 in the simulation without assimilation SW (Fig. 8e).

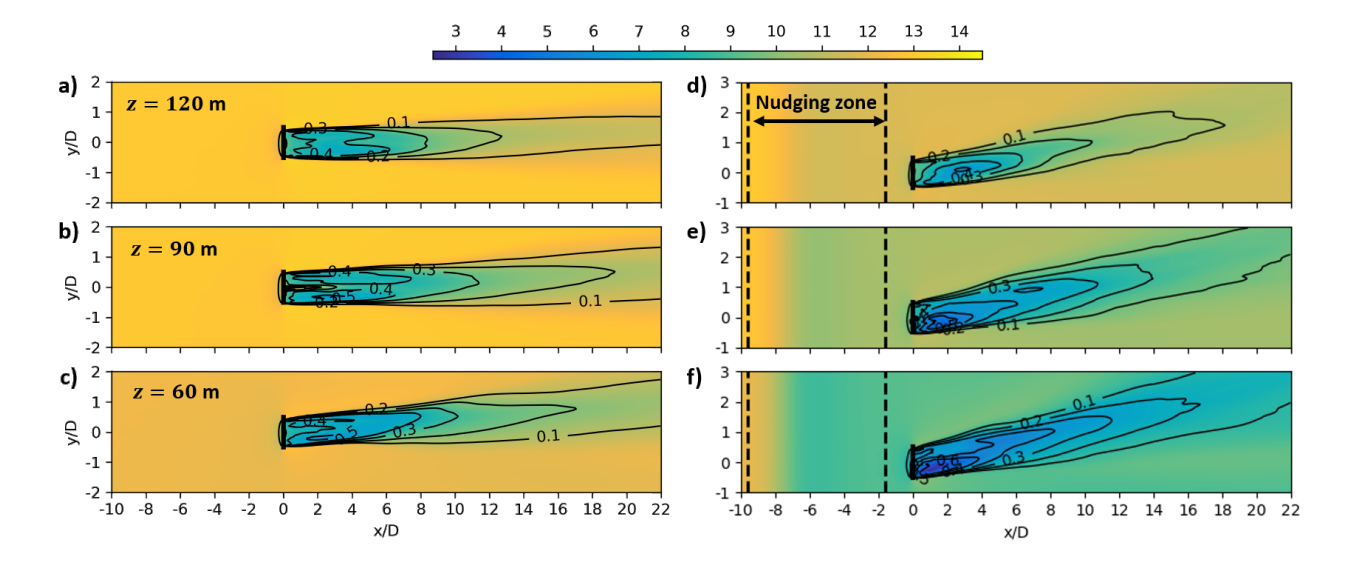


Figure 8. Coloured contours of the time-averaged streamwise zonal velocity component $\overline{u_{i,j,k}}$ in m s⁻¹ without data assimilation in a), b) and c) and with vibration assimilation in d), e) and f) averaged over 20 min at the end of the simulation. b) and e) show the x - y plane at hub height $\frac{1}{2} = 90$ m. a) and d) (c) and f) correspond to the x - y planes at $\frac{1}{2} = 90$ m + $\frac{1}{2}$ correspond to the x - y planes at $\frac{1}{2} = 90$ m + $\frac{1}{2}$ correspond to the x - y planes at $\frac{1}{2} = 90$ m + $\frac{1}{2}$ correspond to the x - y planes at $\frac{1}{2} = 90$ m + $\frac{1}{2}$ correspond to the x - y planes at $\frac{1}{2} = 90$ m + $\frac{1}{2}$ correspond to the x - y planes at $\frac{1}{2} = 90$ m + $\frac{1}{2}$ correspond to the x - y planes at $\frac{1}{2} = 90$ m + $\frac{1}{2}$ correspond to the x - y planes at $\frac{1}{2} = 90$ m + $\frac{1}{2}$ correspond to the x - y planes at $\frac{1}{2} = 90$ m + $\frac{1}{2}$ correspond to the x - y planes at $\frac{1}{2} = 90$ m + $\frac{1}{2}$ correspond to the x - y planes at $\frac{1}{2} = 90$ m + $\frac{1}{2}$ correspond to the x - y planes at $\frac{1}{2} = 90$ m + $\frac{1}{2} = 90$ m + $\frac{1}{2} = 120$ m at the same vertical location calculated in relation to the upstream velocity at $\frac{1}{2} = -200$ m. The axes are normalized by the rotor diameter $\frac{1}{2} = -200$ m, whereby $\frac{1}{2} = -200$ m indicates the position of the rotor.

Also above and beneath hub height the streamwise wake extension is reduced for the simulations with the assimilation method (Fig. 8d and f).—a). However, higher velocity deficit values are reached at the same downwind distance (20 % at x/D = 12-13).

845

850

855

One reason for the reduced wake extension is the lower streamwise wind speed of the assimilated inflow. Another finding is that the turbulence in the wake is higher when the assimilation method is applied. We have already shown in Sect. ?? that the is increased behind the nudging area due to stronger shear and veer in the atmosphere. It is therefore consistent that the turbulence is also higher behind the wind turbine. This effect leads to a more rapid recovery of the wake behind the wind turbine. This effect has already been observed by Englberger and Dörnbrack (2018). higher entrainment in the upper part of the rotor due to significantly increased vertical gradients of the zonal and meridional velocity components (Fig. 6 a, b). Another reason is the pitch angle of the blades which is 3.5° for a hub height wind speed $\bar{u} = 12-13$ m s⁻¹ in simulation SW while it is 0° for $\bar{u} < 12$ m s⁻¹ in simulation SOW. The blades of the wind turbine in the assimilated flow field impose higher tangential and axial forces on the flow field. Further, these reasons are also responsible for the maximum velocity deficit difference in the near wake. It is 60% in simulation SOW in Fig. 8 e) and f), while it reaches only 50% in simulation SO in Fig. 8 b) and c).

Figure 9 a) and c) show the lateral view on a vertical plane through the center of the wind turbine with the visualization of the time-averaged streamwise zonal velocity component \overline{u} . The figure shows that the velocity deficit in the wake is very similar for both simulations in the proximity of the rotoruntil x < 10D. Further downstream the reduced

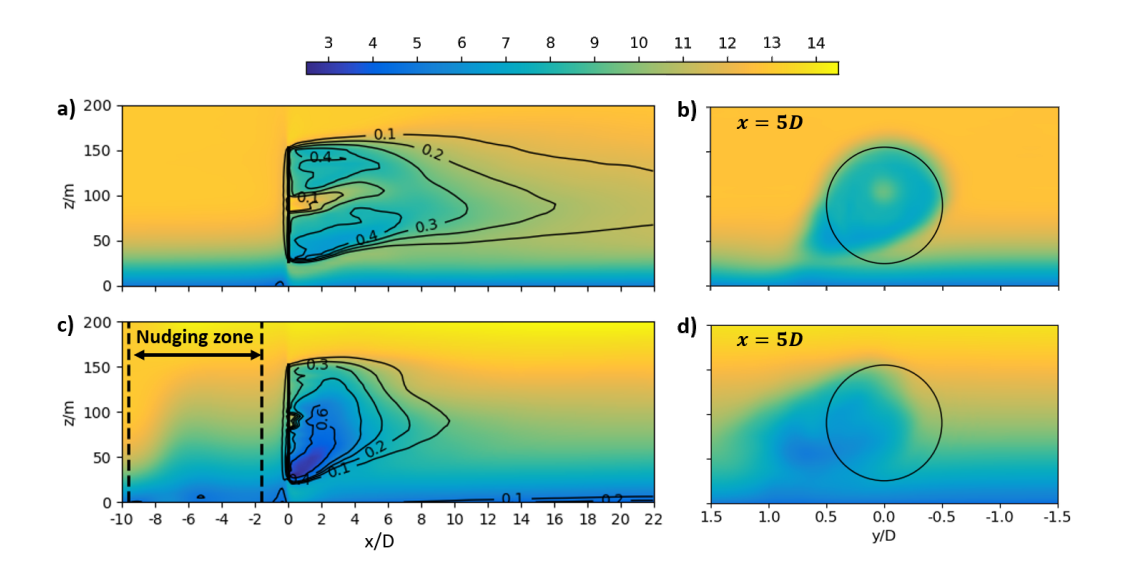


Figure 9. Coloured contours of the time-averaged streamwise zonal velocity component $\overline{u_{i,j_0,k}}$ in m s⁻¹ without assimilation in a) and b) and with vibration assimilation in c) and d) averaged over 20 min at the end of the simulation. In a) and c) the vertical x - z plane at the position y=0 y=0 perpendicular to the turbine is presented. The black contours represent the velocity deficit $VD_{i,j_0,k}$ at the same spanwise location calculated in relation to the upstream velocity at $\frac{x}{x}=-200x=-200$ m. The abscissa is divided by the diameter of the rotor, whereby $\frac{x}{D}=0$ indicates the position of the rotor. b) and d) show streamwise zonal velocity component at a downward position of x=5D. The black circles represent the rotor area.

wake extension is seen for the simulation with assimilation of the velocities (Fig. 9c). Figures 8 and 9 show the interaction Figure 9 b) and d) present a downstream view on the wake at x = 5D behind the rotor. Only a part of the wake is seen in Figure 9 c) due to the deflection of the wake behind the rotor with a stable atmospheric boundary layer flow. The results for both simulations are in good accordance to other studies from Bhaganagar and Debnath (2014), Abkar and Porté-Agel (2015) and Englberger and Dörnbrack (2018) who considered wind-turbine wakes in s. The applied assimilation method changes wind veer and shear in the atmospheric flow. The changed wake structure can also be seen in a downstream view at x = 5D in Fig. 9b and d. While the spanwise wind speed was predominant out of this x-z-plane. While the meridional wind component was predominant only in the lower section of the rotor in the reference case (Fig. 9 9 b) the assimilated wind veer (cf. Fig. 6 b) leads to a deflection of the wake for $z > z_{hub}$ over the whole rotor height (Fig. 9 9 d). In both cases, the wakes respond to the prevalent veer with a stretching of the wake from a circular shaped one towards an ellipsoidal shaped one, which is characteristic under veering inflow conditions.

860

865

870

The streamwise is shown in Fig. ?? for different distances upstream and downstream of the rotor normalized by the mean streamwise velocity at hub height. The influence of the assimilation method can be seen comparing the plots for the distances x/D = -10 and x/D = -1 as the is increased behind the nudging zone. For the analysis of the downstream regions in the simulation with assimilation the at the position x/D = -1 is subtracted in order to separate the induced by the rotor from This

section presented the interaction of the wake behind the rotor within a stable atmospheric boundary-layer flow. The results for both simulations are in good accordance to other studies from Bhaganagar and Debnath (2014), Abkar and Porté-Agel (2015) and Englberger and Dörnbrack (2018) who considered wind-turbine wakes in SBLs. The applied vibration method adapts the wind profile to the target profile and changes wind veer and shear in the atmospheric flow accordingly. Due to these changes of the induced by the assimilation method. At hub height and above the hub an increase of the streamwise can be seen in the near wake until $x/D \le 3$ for the case with nudging. In the reference case the intensity increases slightly over the whole rotor. The for $5 \le x/D \le 10$ increases further for the reference case over the whole rotor area. In the simulation with nudging the beneath hub height is very similar to the in the reference case but it is about two times higher above the hub. For a distance of x/D = 20 the decreases in the simulation with data assimilation as the wake already dissolves. In the far wake for x/D > 10the s match very well for the two simulations. The elevated in the nudging simulation until x/D = 10 leads to the more rapidly recovery of the wake behind the wind turbine which were seen in Fig. 8 and 9c. mean inflow conditions, the developed wake is different in its shape and also considering the velocity deficit compared to the reference case without assimilation. Currently, there is no measurement data available for wakes behind the wind turbines at the wind-farm site at Krummendeich Wi Valdi for the considered situation. Therefore, no a more quantitative analysis of the wake which is shown in this study could not be done at this point. The characteristics of the wake in the near stably stratified boundary layer are accordingly to comparable studies in the literature. The differences in the wake compared to the reference case without nudging can be explained by the changes in the inflow field. It has been proven in this chapter that the vibration assimilation method is capable of changing the inflow velocities towards realistic target velocity profiles for wind turbine simulations.

Comparison of vertical profiles of the streamwise turbulence intensity $\sqrt{u'u'}/\overline{u}_{hub}$ for different distances upstream and downstream of the rotor normalized by the rotor diameter D=126 m. The black solid curves refer to the reference simulation without assimilation. The gray dashed lines refer to the in the simulation with nudging and the red dashed lines show the the induced by the WT (minus TI at x/D=-1 with assimilation). The hub height is marked with the black dashed dotted line and the top tip and bottom tip with the black dashed lines.

7 Conclusions

875

880

885

890

895

900

905

The A systematic sensitivity study with LESs investigating the impact of two versions of Newtonian relaxation and a vibration method on a coarse (spatial resolution of 40 m) and a fine (spatial resolution of 5 m) numerical grid has been performed for an NBL. The coarse resolution results are compatible with the previous study of Nakayama and Takemi (2020). With the fine resolution simulations, the differences of the two Newtonian relaxation methods and the vibration method could be investigated in detail, showing a very similar performance in adjusting the horizontal mean wind to the target velocity profile. In the case of the Newtonian and the vibration approach, the TKE as well as the power spectra are influenced by the relaxation, whereas the 3 D turbulent structures are preserved. The impact of the vibration method in the spectra sets in more slowly in comparison to a more abrupt transition with Newtonian relaxation. This results in a TKE difference compared to the inflow, which is less pronounced when using the vibration method. Therefore, the data assimilation technique using the vibration equation was

validated for the numerical code EULAG and sensitivity studies in regard to gridrefinement were conducted. The vibration assimilation method was applied to assimilate idealized precursor simulations towards measured target wind profiles achieved the most reliable results and could be successfully validated on a fine grid, necessary in wind-energy applications.

910

915

920

925

930

935

940

The vibration method has been applied with a frequency of $f_0 = 0.002 \text{ s}^{-1}$ to adjust velocities from an idealized precursor simulation towards a measured wind profile for the wind farm site WiValdiat Krummendeich. This. In particular, at heights below 60 m, the target profile obtained by measurement data is supplemented by data extracted from a mesoscale model simulation. The resulting ABL with assimilated wind speeds was profiles were used as inflow for the 5MW NREL wind turbine to test the applicability of the vibration method in combination with a rotor. The developed wake and its interaction with the stably stratified boundary layer flow were investigated. The present study contributes to the efficient integration of observational data into under two inflow conditions, the pure precursor inflow and the assimilated inflow, was compared and analysed regarding the temporal averaged zonal wind and the velocity deficit, resulting in a consistent wake pattern. The differences arise mainly from the different horizontal velocity values of the vertical profiles in the precursor simulation in comparison to the measured profile. The present study provides a first insight of the vibration assimilation method of mean velocities and the consecutive response on turbulence characteristics in LES s in order to generate realistic atmospheric for the generation of inflow fields for wind-turbine simulations, wind turbines.

The comparative analysis of the implemented vibration assimilation method with the Newtonian relaxation for a coarse grid spacing method with both Newtonian methods has shown the differences and advantages of the new implemented method. We can now answer the question if the both relaxation methods are different impact on turbulence statistics. Based on the results achieved, the first research question can be answered: Which of the assimilation methods used is able to preserve turbulence in . The use of the Newtonian Relaxation technique is not appropriate for wind-energy purposes because of the severe decrease of atmospheric turbulence in the simulations. Especially for a fine grid the vibration assimilation method showed a better performance in regard to the atmospheric turbulence. We have found that a smaller frequency in the vibration equation within the scope of the defined conditions? We conclude that all assimilation approaches modify the simulated turbulence. The local Newtonian relaxation leads to a lesser decrease of . The presented vibration assimilation method is therefore eapable to assimilate the atmospheric inflow towards target profiles for wind-energy purposes. For an efficient and robust use of the vibration assimilation technique it is necessary that a single precursor simulation can be adapted to an arbitrary target velocity profile. Hence, computational resources can be saved and long and expensive simulations which need to match anticipated characteristics in the can be avoided. The vibration assimilation method changed the mean velocity profiles of the idealized precursor simulations to measured profiles for the wind-farm site WiValdi. The concurrent adaption of the shows that laminarization of the flow. In contrast, Newtonian relaxation and the vibration methods amplify the turbulent perturbations. Although none of the methods tested perfectly preserves the turbulence of the inflow, the methods that do not lead to complete decay are therefore preferable. There is the potential to improve the method further to more closely assimilate to the inflow turbulence. For the Newtonian method, Allaerts et al. (2020, 2023) did a first step into this direction. A similar approach is necessary for the vibration method in future.

In this work, two different highly resolved precursor simulations are applied. We found that the vibration method represents turbulencegenerating processes which occur when the idealized is transformed into a more realistic boundary layer. The importance of the consideration of the atmospheric stratification (lapse rate) has been presented. The vibration assimilation method is only successful applicable when the basic atmospheric stratification in the precursor simulation conditions and the target profile agree and the main characteristics of the wind conditions match (e.g. wind veer). This study has shown that for wind energy purposes it is not sufficient to consider only the lowest 300 m of the atmosphere but rather the whole boundary layer height. For the assimilation of velocities in atmospheric precursor simulations towards realistic wind profiles it is hence necessary, that the stratification of the atmosphere in the precursor simulation is similar to the conditions in the boundary layer in which the observations are performed, are relatively close to each other in structure, e.g. either veering inflow or pure zonal flow. It was not possible to assimilate a precursor simulation with no meridional wind component to a veering target profile. These results of the numerical simulations answer our second research question, namely whether velocities taken from precursor simulations of idealized atmospheric flows can be assimilated towards arbitrary measured wind profiles. In these arbitrary profiles there must be a vertical gradient of the meridional wind. Since only one precursor simulation has to be performed to adapt the simulated velocities to different expected target profiles of ABL flows, the presented numerical setup has the ultimate advantage of saving computational resources for long and expensive simulations.

945

950

955

960

965

970

975

Finally, the assimilated flow field was used as inflow for a wind turbine which is simulation which was parameterized with the blade element momentum method as rotating actuator disc. The, providing an answer to the third research question of how the wake behind a wind turbines changes if velocities of idealized inflow conditions are assimilated. The differences in the wake behind the wind turbine in (wake deflection, wake elongation, velocity deficit) performed with the assimilated flow field showed well known structures and intensity profiles. In general, in comparison to the one with the inflow of the non-assimilated pure precursor simulation, can be traced back to the differences in the horizontal mean of the inflow velocities (e.g., increase of vertical gradient of zonal and meridional flow). The wake structures (ellipsoidal in lateral cross section, wake deflection due to wind direction changing with height) are in agreement with many previous publications (e.g. Abkar et al., 2016; Vollmer et al., 2016; Bhaganagar and Debnath, 2014; Englberger and Dörnbrack, 2018). The assimilation itself did not influence these structures as it was to be expected from the fact that the discussed effects on the wake evoked by the nudging method are reasonable. It must be said that at the moment of the vibration method only adapts the mean value of the wind speed, while attaining the turbulent 3D structures. This result makes the vibration method suitable and attractive for wind-turbine simulations. The DWL-measurements at Krummendeich the that were used in this study were taken at a time when wind turbines were still under construction and measurement data of the wake are at the WiValdi windpark, so that measurement data for wind turbine wakes is not available for this time in order to provide a comparative analysis in this study. In conclusion, the presented vibration assimilation method can assimilate atmospheric inflow fields for wind energy purposes. Arbitrary velocity profiles for a specified atmospheric stratification can be reproduced by the developed model. The conditions in the precursor simulation and the target wind profiles must show similar characteristics for a successful result of the assimilation method. Further tests with different atmospheric stratifications and more observational data will be conducted and presented at the TOROUE 2024 (Wrba et al. (2024)). As soon as measurement data of the wake behind the wind turbine at

the wind-farm site WiValdi is available, a comparative analysis of the computed wake in EULAG and the wake measurements is possible. with observations. A logical next step would be to extend the current work by assimilating to a profile at a time in which nacelle-based lidar wake measurements are available also (since November, 2023).

Our setup offers two advantages when compare to the setup of Allaerts et al. (2020) and Allaerts et al. (2023): Our setup has the possibility to assimilate simultaneous (time varying) measurements, as it works with open horizontal boundary conditions. Further, it is basically applicable in complex terrain. Its value in these areas has to be tested in future studies, but the general requirements are fulfilled.

Appendix A: WRF Setup

980

985

990

995

1000

The wind profiles used as target velocity profiles in Sect. 5 and Sect. 6 were extracted from a simulation using performed with the WRF model version 4.4.1. A particular time period during 19.11.2021 was chosen from DWL-observations taken at the research wind farm located at Krummendeich (cf. Sect. 2.3). On this day the DWL-observations showed that the conditions at the wind park represented a quasi-neutral boundary layer with nominal wind speeds at hub height of roughly 10 m s⁻¹. The WRF simulation consists of four nested domains, with a horizontal grid spacing of 5 km, 1 km, 200 m and 40 m for domains 1-4, respectively. The domains with sub-kilometer grid spacing are run in LES mode. Vertical nesting is applied also, so that higher vertical resolution is used in the domains with higher horizontal resolution. The mean target profiles for the streamwise and spanwise-zonal and meridional velocity used in EULAG are extracted from D4 and vertically interpolated so that there is a constant dz = 5 m. Initial and boundary conditions are supplied from the European Centre for Medium-Range Weather Forecasts (ECMWF) operational analyses, which has a temporal resolution of 6 h. Topography data for the LES domains are provided by the Copernicus digital elevation model and are available at a horizontal grid spacing of 90 m and 30 m. The model top was set at about 12 km height to include tropopause effects. A 3 km upper damping layer is implemented, to restrict reflection of gravity waves. The Monin-Obukhov scheme is used to simulate the surface layer (Janjic (1996)). Additionally, the Noah-MP land-surface model (Niu et al. (2011)), the Rapid Radiative Transfer Model long-wave scheme (Mlawer et al. (1997)), the Dudhia short-wave scheme (Dudhia (1989)), the WRF single-moment five-class microphysics scheme (Hong and Lim (2006)) are used. In domains 1 and 2 the Kain-Fritsch cumulus parameterization scheme is implemented (Kain and Fritsch (1990)) and a planetary boundary scheme is used, namely the Mellor-Yamada-Janjic TKE scheme (Mellor and Yamada (1982)). In the LES domains (domains 3-4) the cumulus parameterization and planetary boundary schemes are switched off, and SGS turbulence is parameterized by a three-dimensional 1.5-order TKE closure (Deardorff (1980)). The simulations were performed for a total of 7 hours, from 12 UTC to 19 UTC on 19.11.2021.

Author contributions. All authors conceived the idea and contributed to the manuscript. LW performed the simulations and visualisation.

1005 LW and AE did the conceptual design. NW performed the DWL and MWR measurements and GK computed the WRF simulation.

Competing interests. The contact author has declared that neither of the authors has any competing interests.

1010

Acknowledgements. Measurements at the WiValdi research park (https://windenergy-researchfarm.com/) were conducted as part of the research project Deutsche Forschungsplattform für Windenergie (http://dfwind.de). We greatly acknowledge the financial support of the German Federal Ministry for Economic Affairs and Climate Action, through FKZ 0325936, that enabled this work. The authors gratefully acknowledge the Gauss Centre for Supercomputing e.V. (http://www.gauss-center. eu) for funding this project by providing computing time on the GCS Supercomputer SuperMUC at Leibniz Supercomputing Centre (LRZ, www.lrz.de). Funding was provided by German Aerospace Center (DLR e.V.).

References

- Abkar, M. and Porté-Agel, F.: Influence of atmospheric stability on wind-turbine wakes: A large-eddy simulation study, Physics of fluids, 27, 035 104, https://doi.org/10.1063/1.4913695, 2015.
 - Abkar, M., Sharifi, A., and Porté-Agel, F.: Wake flow in a wind farm during a diurnal cycle, Journal of Turbulence, 17, 420-441, 2016.
 - Aitken, M. L., Kosović, B., Mirocha, J. D., and Lundquist, J. K.: Large eddy simulation of wind turbine wake dynamics in the stable boundary layer using the Weather Research and Forecasting Model, Journal of Renewable and Sustainable Energy, 6, 2014.
- Allaerts, D., Quon, E., Draxl, C., and Churchfield, M.: Development of a time–height profile assimilation technique for large-eddy simulation, Boundary-Layer Meteorology, 176, 329–348, 2020.
 - Allaerts, D., Quon, E., and Churchfield, M.: Using observational mean-flow data to drive large-eddy simulations of a diurnal cycle at the SWiFT site, Wind Energy, 26, 469–492, 2023.
 - Arcucci, R., D'Amore, L., Pistoia, J., Toumi, R., and Murli, A.: On the variational data assimilation problem solving and sensitivity analysis, Journal of Computational Physics, 335, 311–326, 2017.
- Bhaganagar, K. and Debnath, M.: Implications of Stably Stratified Atmospheric Boundary Layer Turbulence on the Near-Wake Structure of Wind Turbines, Energies, 7, 5740–5763, https://doi.org/10.3390/en7095740, 2014.
 - Bhaganagar, K. and Debnath, M.: The effects of mean atmospheric forcings of the stable atmospheric boundary layer on wind turbine wake, Journal of Renewable and Sustainable Energy, 7, 013 124, https://doi.org/10.1063/1.4907687, 2015.
- Chanprasert, W., Sharma, R., Cater, J., and Norris, S.: Large Eddy Simulation of wind turbine wake interaction in directionally sheared inflows, Renewable Energy, 201, 1096–1110, 2022.
 - Deardorff, J. W.: Three-dimensional numerical study of turbulence in an entraining mixed layer, Boundary-Layer Meteorology, 7, 199–226, https://doi.org/10.1007/BF00227913, 1974.
 - Deardorff, J. W.: Stratocumulus-capped mixed layers derived from a three-dimensional model, Boundary-layer meteorology, 18, 495–527, 1980.
- Dudhia, J.: Numerical study of convection observed during the winter monsoon experiment using a mesoscale two-dimensional model, Journal of Atmospheric Sciences, 46, 3077–3107, 1989.
 - Dörnbrack, A.: Transient Tropopause Waves, Journal of the Atmospheric Sciences, https://doi.org/10.1175/JAS-D-24-0037.1, 2024.
 - Elliott, J. R. and Smolarkiewicz, P. K.: Eddy resolving simulations of turbulent solar convection, International Journal for Numerical Methods in Fluids, 39, 855–864, 2002.
- Englberger, A. and Dörnbrack, A.: Impact of neutral boundary-layer turbulence on wind-turbine wakes: a numerical modelling study, Boundary-Layer Meteorology, 162, 427–449, https://doi.org/10.1007/s10546-016-0208-z, 2017.
 - Englberger, A. and Dörnbrack, A.: Impact of the Diurnal Cycle of the Atmospheric Boundary Layer on Wind-Turbine Wakes: A Numerical Modelling Study, Boundary Layer Meteorology, https://doi.org/10.1007/s10546-017-0309-3, 2018.
 - Hansen, M.: Aerodynamics of Wind Turbines, Earthscan, https://books.google.de/books?id=GVD_HDPix6YC, 2013.
- Haupt, S. E., Kosovic, B., Berg, L. K., Kaul, C. M., Churchfield, M., Mirocha, J., Allaerts, D., Brummet, T., Davis, S., DeCastro, A., et al.: Lessons learned in coupling atmospheric models across scales for onshore and offshore wind energy, Wind Energy Science Discussions, 2022, 1–36, 2022.

- Heinze, R., Moseley, C., Böske, L. N., Muppa, S. K., Maurer, V., Raasch, S., and Stevens, B.: Evaluation of large-eddy simulations forced with mesoscale model output for a multi-week period during a measurement campaign, Atmospheric Chemistry and Physics, 17, 7083–7109, 2017.
 - Hong, S.-Y. and Lim, J.-O. J.: The WRF single-moment 6-class microphysics scheme (WSM6), Asia-Pacific Journal of Atmospheric Sciences, 42, 129–151, 2006.
 - Janjic, Z.: The Mellor-Yamada level-2.5 scheme in the NCEP Eta model, in: Preprint, 11[<] th> AMS Conference on Numerical Weather Prediction, Norfolk, VA, 1996, 1996.
- Jonkman, J., Butterfield, S., Musial, W., and Scott, G.: Definition of a 5-MW Reference Wind Turbine for Offshore System Development, https://doi.org/10.2172/947422, 2009.
 - Kain, J. S. and Fritsch, J. M.: A one-dimensional entraining/detraining plume model and its application in convective parameterization, Journal of Atmospheric Sciences, 47, 2784–2802, 1990.
- Kilroy, G., Englberger, A., Wrba, L., Bührend, L., and Wildmann, N.: Evaluation of turbulence characteristics in WRF simulations at WiValdi wind park, Journal of Physics: Conference Series, 2767, 052 063, https://doi.org/10.1088/1742-6596/2767/5/052063, 2024.
 - Lilly, D. K.: On the computational stability of numerical solutions of time-dependent non-linear geophysical fluid dynamics problems, Monthly Weather Review, 93, 11–25, 1965.
 - Lu, H. and Porté-Agel, F.: Large-eddy simulation of a very large wind farm in a stable atmospheric boundary layer, Physics of Fluids, 23, 2011.
- 1065 Mann, J.: The spatial structure of neutral atmospheric surface-layer turbulence, Journal of fluid mechanics, 273, 141–168, https://doi.org/10.1017/S0022112094001886, 1994.
 - Margolin, L. G., Smolarkiewicz, P. K., and Sorbjan, Z.: Large-eddy simulations of convective boundary layers using nonoscillatory differencing, Physica D: Nonlinear Phenomena, 133, 390–397, 1999.
- Maronga, B., Gryschka, M., Heinze, R., Hoffmann, F., Kanani-Sühring, F., Keck, M., Ketelsen, K., Letzel, M. O., Sühring, M., and Raasch,
 S.: The Parallelized Large-Eddy Simulation Model (PALM) version 4.0 for atmospheric and oceanic flows: model formulation, recent developments, and future perspectives, Geoscientific Model Development, 8, 2515–2551, 2015.
 - Mellor, G. L. and Yamada, T.: Development of a turbulence closure model for geophysical fluid problems, Reviews of Geophysics, 20, 851–875, 1982.
- Mirocha, J., Kosovic, B., Aitken, M., and Lundquist, J.: Implementation of a generalized actuator disk wind turbine model into the weather research and forecasting model for large-eddy simulation applications, Journal of Renewable and Sustainable Energy, 6, 013 104, https://doi.org/10.1063/1.4861061, 2014.
 - Mixa, T., Dörnbrack, A., and Rapp, M.: Nonlinear Simulations of Gravity Wave Tunneling and Breaking over Auckland Island, Journal of the Atmospheric Sciences, 78, 1567 1582, https://doi.org/10.1175/JAS-D-20-0230.1, 2021.
- Mlawer, E. J., Taubman, S. J., Brown, P. D., Iacono, M. J., and Clough, S. A.: Radiative transfer for inhomogeneous atmospheres: RRTM, a validated correlated-k model for the longwave, Journal of Geophysical Research: Atmospheres, 102, 16663–16682, 1997.
 - Nakayama, H. and Takemi, T.: Development of a Data Assimilation Method Using Vibration Equation for Large-Eddy Simulations of Turbulent Boundary Layer Flows, Journal of Advances in Modeling Earth Systems, 12, e2019MS001 872, 2020.
 - Nakayama, H., Takemi, T., and Nagai, H.: Large-eddy simulation of urban boundary-layer flows by generating turbulent inflows from mesoscale meteorological simulations, Atmospheric Science Letters, 13, 180–186, 2012.

- Nakayama, H., Leitl, B., Harms, F., and Nagai, H.: Development of local-scale high-resolution atmospheric dispersion model using large-eddy simulation. Part 4: turbulent flows and plume dispersion in an actual urban area, Journal of Nuclear Science and Technology, 51, 626–638, 2014.
- Nakayama, H., Takemi, T., and Nagai, H.: Development of LO cal-scale H igh-resolution atmospheric DI spersion M odel using L arge-E ddy S imulation. Part 5: detailed simulation of turbulent flows and plume dispersion in an actual urban area under real meteorological conditions, Journal of Nuclear Science and Technology, 53, 887–908, 2016.
 - Naughton, J., Balas, M., Gopalan, H., Gundling, C., Heinz, S., Kelly, R., Lindberg, W., Rai, R., Saini, M., and Sitaraman, J.: Turbulence and the isolated wind turbine, in: 6th AIAA theoretical fluid mechanics conference, p. 3612, 2011.
 - Neggers, R. A., Siebesma, A., and Heus, T.: Continuous single-column model evaluation at a permanent meteorological supersite, Bulletin of the American Meteorological Society, 93, 1389–1400, 2012.
- Niu, G.-Y., Yang, Z.-L., Mitchell, K. E., Chen, F., Ek, M. B., Barlage, M., Kumar, A., Manning, K., Niyogi, D., Rosero, E., et al.: The community Noah land surface model with multiparameterization options (Noah-MP): 1. Model description and evaluation with local-scale measurements, Journal of Geophysical Research: Atmospheres, 116, 2011.
 - Porté-Agel, F., Bastankhah, M., and Shamsoddin, S.: Wind-turbine and wind-farm flows: A review, Boundary-layer meteorology, 174, 1–59, 2020.
- Prusa, J. M., Smolarkiewicz, P. K., and Wyszogrodzki, A. A.: EULAG, a computational model for multiscale flows, Computers and Fluids, 37, 1193–1207. https://doi.org/https://doi.org/10.1016/i.compfluid.2007.12.001, 2008.
 - Rohli, R. V. and Li, C.: Atmospheric Stability and Potential Temperature, pp. 77–90, Springer International Publishing, Cham, https://doi.org/10.1007/978-3-030-73093-2_8, 2021.
- Sanchez Gomez, M. and Lundquist, J. K.: The effect of wind direction shear on turbine performance in a wind farm in central Iowa, Wind Energy Science, 5, 125–139, 2020.
 - Skamarock, W. C., Klemp, J. B., Dudhia, J., Gill, D. O., Liu, Z., Berner, J., Wang, W., Powers, J., Duda, M., Barker, D., et al.: A description of the advanced research WRF version 4, NCAR tech. note ncar/tn-556+ str, 145, 2019.
 - Smolarkiewicz, P. K. and Dörnbrack, A.: Conservative integrals of adiabatic Durran's equations, International journal for numerical methods in fluids, 56, 1513–1519, 2008.
- 1110 Smolarkiewicz, P. K. and Margolin, L. G.: MPDATA: A Finite-Difference Solver for Geophysical Flows, Journal of Computational Physics, 140, 459–480, https://doi.org/https://doi.org/10.1006/jcph.1998.5901, 1998.
 - Smolarkiewicz, P. K. and Margolin, L. O.: On forward-in-time differencing for fluids: Extension to a curvilinear framework, Monthly Weather Review, 121, 1847–1859, 1993.
- Smolarkiewicz, P. K. and Pudykiewicz, J. A.: A class of semi-Lagrangian approximations for fluids, Journal of Atmospheric Sciences, 49, 2082–2096, 1992.
 - Smolarkiewicz, P. K., Sharman, R., Weil, J., Perry, S. G., Heist, D., and Bowker, G.: Building resolving large-eddy simulations and comparison with wind tunnel experiments, Journal of Computational Physics, 227, 633–653, https://doi.org/https://doi.org/10.1016/j.jcp.2007.08.005, 2007.
- Spille-Kohoff, A. and Kaltenbach, H.-J.: Generation of turbulent inflow data with a prescribed shear-stress profile, in: DNS/LES Progress and Challenges, edited by Liu, C., Sakell, L., and Beutner, T., pp. pp. 319–326, Greyden Press, 2001.
 - Stauffer, D. R. and Seaman, N. L.: Use of four-dimensional data assimilation in a limited-area mesoscale model. Part I: Experiments with synoptic-scale data, Monthly Weather Review, 118, 1250–1277, 1990.

- Stull, R. B.: An introduction to boundary layer meteorology, 2003.
- Troldborg, N., Sørensen, J. N., and Mikkelsen, R.: Actuator line simulation of wake of wind turbine operating in turbulent inflow, in: Journal of physics: conference series, vol. 75, p. 012063, IOP Publishing, 2007.
 - Veers, P., Bottasso, C. L., Manuel, L., Naughton, J., Pao, L., Paquette, J., Robertson, A., Robinson, M., Ananthan, S., Barlas, T., et al.: Grand challenges in the design, manufacture, and operation of future wind turbine systems, Wind Energy Science, 8, 1071–1131, 2023.
 - Vollmer, L., Steinfeld, G., Heinemann, D., and Kühn, M.: Estimating the wake deflection downstream of a wind turbine in different atmospheric stabilities: an LES study, Wind Energy Science, 1, 129–141, https://doi.org/10.5194/wes-1-129-2016, 2016.
- 1130 Wharton, S. and Lundquist, J. K.: Atmospheric stability affects wind turbine power collection, Environmental Research Letters, 7, 014 005, https://doi.org/10.1088/1748-9326/7/1/014005, 2012.
 - Wildmann, N., Päschke, E., Roiger, A., and Mallaun, C.: Towards improved turbulence estimation with Doppler wind lidar velocity-azimuth display (VAD) scans, Atmospheric Measurement Techniques, 13, 4141–4158, https://doi.org/10.5194/amt-13-4141-2020, 2020.
 - Wildmann, N., Hagen, M., and Gerz, T.: Enhanced resource assessment and atmospheric monitoring of the research wind farm WiValdi, in: Journal of Physics: Conference Series, vol. 2265, p. 022029, IOP Publishing, 2022.
 - WiValdi: https://windenergy-researchfarm.com.

1135

Wrba, L., Bührend, L., Englberger, A., Dörnbrack, A., and Widmann, N.: A stably-stratified atmospheric inflow assimilated to measured mean profiles interacting with a wind park, Conference Paper TORQUE 2024, 2024.